Center for Environmentally Sustainable Transportation

A Bio-Wicking System to Mitigate Capillary Water in Base Course

Chuang Lin, Graduate Research Assistant
Xiong Zhang, Ph.D., P.E.
Department of Civil and Environmental Engineering
University of Alaska Fairbanks

Date: November 2016

Prepared by:

Center for Environmentally Sustainable
Transportation in Cold Climates
Duckering Building, Room 245
P.O. Box 755900
Fairbanks, AK 99775

INE/AUTC 17.01

REPORT DOCUMENTATION PAGE

Form approved OMB No.

1. AGENCY USE ONLY (LEAVE BLANK)	2. REPORT DATE	3. REPORT TYPE AND DATES COVERED
	11/2016	Final Report: 06/2014 – 12/2016

4. TITLE AND SUBTITLE

A Bio-Wicking System to Mitigate Capillary Water in Base Course

5. FUNDING NUMBERS

6. AUTHOR(S)

Chuang Lin, Graduate Research Assistant
Xiong Zhang, Ph.D., P.E.
University of Alaska Fairbanks

7. PERFORMING ORGANIZATION NAME(S) AND ADDRESS(ES)

Center for Environmentally Sustainable Transportation in Cold Climates
University of Alaska Fairbanks
Duckering Building, Room 245
P.O. Box 755900
Fairbanks, AK 99775-5900

8. PERFORMING ORGANIZATION REPORT NUMBER

9. SPONSORING/MONITORING AGENCY NAME(S) AND ADDRESS(ES)

TenCate Geosynthetics
365 South Holland Drive
Pendergrass, GA 30567

10. SPONSORING/MONITORING AGENCY REPORT NUMBER

11. SUPPLENMENTARY NOTES

12a. DISTRIBUTION / AVAILABILITY STATEMENT

No restrictions

12b. DISTRIBUTION CODE

13. ABSTRACT (Maximum 200 words)

Water within pavement layers is the major cause of pavement deteriorations. High water content results in significant reduction in soil's resilient behavior and increase in permanent deformation. Conventional drainage systems can only drain gravity water but not capillary water. Both preliminary lab and field tests have proven the drainage efficiency of a newly developed H2Ri geotextile with wicking fabrics. This bio-wicking system aims at resolving the potential issues that the original design may encounter: (1) H2Ri ultraviolet degradation, (2) H2Ri mechanical failure, (3) loss of drainage function under high suction, and (4) clogging and salt concentration.

Both elemental level and full-scale test results indicated that the bio-wicking system is more effective in draining capillary water within the base courses compared with original design, in which the geotextile is directly exposed to the open air. However, a good drainage condition is required for the bio-wicking system to maintain its drainage efficiency. Accumulation of excess water will result in water re-entering the road embankment. Moreover, grass root and geotextile share the same working mechanism in transporting water. In the proposed bio-wicking system, the relatively smaller channels in the grass roots further ensures water moving from H2Ri geotextile, transporting through the stems of grass, and eventually evapo-transpiring into the air at the leaf-air interfaces. In sum, the bio-wicking system seemed to successfully address the concerns in the preliminary design and is a more efficient system to dehydrate the road embankment under unsaturated conditions.

14- KEYWORDS : Geotextiles, Subsurface Drainage, Unsaturated Soils, Capillarity, Embankments

15. NUMBER OF PAGES
87

16. PRICE CODE
N/A

17. SECURITY CLASSIFICATION OF REPORT	18. SECURITY CLASSIFICATION OF THIS PAGE	19. SECURITY CLASSIFICATION OF ABSTRACT	20. LIMITATION OF ABSTRACT
Unclassified	Unclassified	Unclassified	N/A

A Bio-Wicking System to Mitigate Capillary Water in Base Course

Final Project Report

By

Chuang Lin, Graduate Research Assistant
Xiong Zhang, Ph.D., P.E.
Associate Professor

Department of Civil and Environmental Engineering
University of Alaska Fairbanks

Project Title: A Bio-Wicking System to Mitigate Capillary Water in Base Course

Performed in cooperation

with

TenCate Geosynthetics (North America)

November 2016

DISCLAIMER

This document is disseminated under the sponsorship of the U.S. Department of Transportation in the interest of information exchange. The U.S. Government assumes no liability for the use of the information contained in this document. The U.S. Government does not endorse products or manufacturers. Trademarks or manufacturers' names appear in this report only because they are considered essential to the objective of the document.

Opinions and conclusions expressed or implied in the report are those of the author(s). They are not necessarily those of the funding agencies. This report does not constitute a standard, specification, or regulation.

METRIC (SI*) CONVERSION FACTORS

APPROXIMATE CONVERSIONS TO SI UNITS

Symbol	When You Know	Multiply By	To Find	Symbol
		LENGTH		
in	inches	25.4		mm
ft	feet	0.3048		m
yd	yards	0.914		m
mi	Miles (statute)	1.61		km
		AREA		
in^2	square inches	645.2	millimeters squared	cm^2 ft^2
	square feet	0.0929	meters squared	m^2
yd^2	square yards	0.836	meters squared	m^2
mi^2	square miles	2.59	kilometers squared	km^2
ac	acres	0.4046	hectares	ha
		MASS (weight)		
oz	Ounces (avdp)	28.35	grams	g lb
	Pounds (avdp)	0.454	kilograms	kg T
	Short tons (2000 lb)	0.907	megagrams	mg
		VOLUME		
fl oz	fluid ounces (US)	29.57	milliliters	mL gal
	Gallons (liq)	3.785	liters	liters ft^3
	cubic feet	0.0283	meters cubed	m^3
yd^3	cubic yards	0.765	meters cubed	m^3
Note: Volumes greater than 1000 L shall be shown in m^3				
		TEMPERATURE (exact)		
ºF temperature	Fahrenheit	5/9 (ºF-32)	Celsius temperature	ºC
		ILLUMINATION		
fc	Foot-candles	10.76	lux	lx
fl	foot-lamberts	3.426	candela/m^2	cd/cm^2
		FORCE and PRESSURE or STRESS		
lbf	pound-force	4.45	newtons	N psi
square inch	pound-force per	6.89	kilopascals	kPa

These factors conform to the requirement of FHWA Order 5190.1A *SI is the symbol for the International System of Measurements

APPROXIMATE CONVERSIONS FROM SI UNITS

Symbol	When You Know	Multiply By	To Find	Symbol
		LENGTH		
mm	millimeters			0.039
inches			in	
m	meters			3.28
feet			ft	
m	meters			1.09
yards			yd	
km	kilometers			0.621
Miles (statute)			mi	
		AREA		
mm^2	millimeters squared		0.0016	square inches
in^2 m^2	meters squared		10.764	square
feet			ft^2 km^2	kilometers squared
0.39	square miles		mi^2 ha	hectares
(10,000 m^2)			2.471	acres
ac				
		MASS (weight)		
g	grams			0.0353
Ounces (avdp)			oz	
kg	kilograms			2.205
Pounds (avdp)			lb mg	megagrams (1000 kg)
1.103	short tons		T	
		VOLUME		
mL	milliliters			0.034
fluid ounces (US)			fl oz	
liters	liters			0.264
Gallons (liq)			gal	
m^3	meters cubed			35.315
cubic feet			ft^3	
m^3	meters cubed			1.308
cubic yards			yd^3	
		TEMPERATURE (exact)		
ºC	Celsius temperature			9/5 ºC+32
Fahrenheit temperature			ºF	
		ILLUMINATION		
lx	lux			0.0929
foot-candles			fc	
cd/cm	candela/m^2			0.2919

ACKNOWLEDGMENTS

The authors wish to express their appreciation to TenCate Geosynthetics (North America) and the Center for Environmentally Sustainable Transportation in Cold Climates (CESTiCC) for their financial support throughout this study. The authors would also like to thank all members of the project advisory committee. Appreciation is extended to Lin Li and Sheng Zhao, whose efforts have contributed to sample collection and laboratory testing processes.

TABLE OF CONTENTS

LIST OF FIGURES

LIST OF TABLES

Executive Summary

Water within pavement layers is a major cause of pavement deterioration. Because conventional drainage systems cannot wholly solve this issue, geosynthetic materials have been adopted to remove water from pavement. Recent studies have shown that geotextiles (either alone or combined with other geosynthetics) may also be used as effective drainage material to substitute for conventional drainage materials in pavement structures. Preliminary tests have demonstrated that, in comparison with conventional geotextiles under unsaturated conditions, H2Ri geotextile with wicking fabric is more efficient at laterally draining out capillary water. A field test section at Beaver Slide along the Dalton Highway in Alaska indicated that H2Ri geotextile successfully eliminates distress caused by frost heave and subsequent thaw weakening. However, H2Ri geotextile has limited ability to hold water despite its ability to wick water from surrounding soils. In its original design, H2Ri must be exposed at the roadside so that water can vaporize to generate the hydraulic gradient that helps maintain constant water transport. This design may cause issues in the long-term performance of pavement during its service life, since (1) H2Ri degrades over time due to sunlight exposure; (2) routine grass mowing maintenance may cause mechanical damage to the geotextile; (3) the geotextile may lose function under high suction conditions due to air intrusion in its drainage channels; and (4) clogging and salt concentration may influence the geotextile's drainage efficiency.

This research involved an investigation into the possibility of a bio-wicking system that addresses the issues just mentioned. The H2Ri geotextile was buried 1–2 in. deep in topsoil at the road shoulder. The road shoulder was then hydro-seeded to establish vegetation so that evaporation would occur at the leaves of the vegetation instead of directly from the wicking

fabric. The vegetation worked as a “pump” to vaporize the water from the soil, while the H2Ri served as a pipe that maintained saturation under negative pore water pressures. Vegetation wilts at a suction of 1500 kPa so that the H2Ri did not become overly dry. This bio-wicking system maintains the benefits of wicking fabric while simplifying maintenance.

Both elemental and full-scale test results indicate that this bio-wicking system is more effective at mitigating capillary water within the base course than the original design, in which the geotextile is directly exposed to open air. However, good drainage is required for the bio-wicking system to maintain its drainage efficiency. Accumulation of excess water results in water flowing in the reverse direction. Moreover, the similarities of the grass and geotextile microstructures indicate that the essential working mechanisms for grass and geotextile are the same. Both take advantage of capillary action and water potential difference (suction gradient) to transport water. The relatively smaller spacing of the grass root drainage path further ensures that water moves from geotextile to grass and eventually evaporates in the air. In summary, the bio-wicking system described in this report successfully solved the potential issues of the original design and is a more efficient system for dehydrating road embankments.

CHAPTER 1.0 INTRODUCTION

1.1 Problem Statement

Water is the main cause of deterioration in pavement structures (Cedergren, 1994). Excess moisture in pavement structures decreases pavement serviceability by more than half (Christopher and McGuffey, 1997). Conventional subsurface drainage design addresses this issue by adding an interlayer drainage system (a permeable aggregate base course under the asphalt layer and an edge drain to divert the water toward drainage pipes). However, this drainage system assumes saturated flow and is not always effective in maintaining the moisture content of unbounded pavement layers (Heckel, 1997). Beskow (1991) found that conventional drainage systems are not wholly effective at reducing water-related problems in partially saturated soils. Soil above the groundwater table is unsaturated, and frost heaves occur through the capillary rise of water. Since pavement structure is rarely saturated, water flow under unsaturated conditions and the unsaturated properties of geomaterials are considered in pavement design procedures.

Recent studies have proved that geotextiles (either alone or combined with other geosynthetics) may be used as effective drainage layers, as a substitute for conventional drainage materials in pavement structures. A new design includes a capillary break and a drainage system that wicks water out of soil, providing drainage while the soil is unsaturated. A typical example of this design is the NCHRP-IDEA Project 68 “Geocomposite barrier drain for limiting moisture changes in pavement subgrades and base courses” (Henry and Stormont, 2002). The key to the success of such a system is the use of a material that has high wettability (which means it can absorb water from unsaturated soils) and high unsaturated permeability (so that it transports the absorbed water out of the pavement structure quickly). While numerous techniques have been

developed to mitigate pavement damage caused by capillary action, improvements are still expected to reduce or eliminate the impact of moisture accumulation (especially capillary water) in a more cost-effective way. The geotextile H2Ri, newly developed by TenCate Geosynthetics, shows great promise as a cost-effective means of controlling moisture migration under unsaturated conditions. Available data and field observations at a test section at Beaver Slide, located along the Dalton Highway in Alaska, clearly show that H2Ri geotextile with wicking fabric successfully eliminates frost boil problems, a typical issue induced by capillary action.

The H2Ri geotextile has limited ability to hold water despite its ability to wick water from surrounding soils. In its original design (see Figure 1.1), H2Ri must be exposed at the roadside so that water can vaporize to generate enough hydraulic gradient to maintain constant water transport. This original design may cause issues when considering the long-term performance of pavement during its service life (usually 20–30 years), since (1) H2Ri degrades with time due to sunlight exposure, (2) air may intrude into the multi-channels of the geotextile and significantly reduce its drainage efficiency, and (3) maintenance may require special techniques that a budget cannot afford.

The authors carried out an investigation into the possibility of using a bio-wicking system (see Figure 1.2). In the modified system, H2Ri was buried about 1–2 in. in topsoil at the road shoulder. The road shoulder was then hydro-seeded to establish vegetation. Using this design, evaporation occurs at the leaves of the vegetation instead of directly from the wicking fabric. The vegetation works as a "pump" to vaporize the water out of the soil, while the H2Ri geotextile serves as a pipe that maintains saturation under negative pore water pressures. The vegetation wilts at a suction of 1500 kPa so that H2Ri does not become overly dry. This bio-wicking system maintains the wicking benefits of wicking fabric while simplifying maintenance.

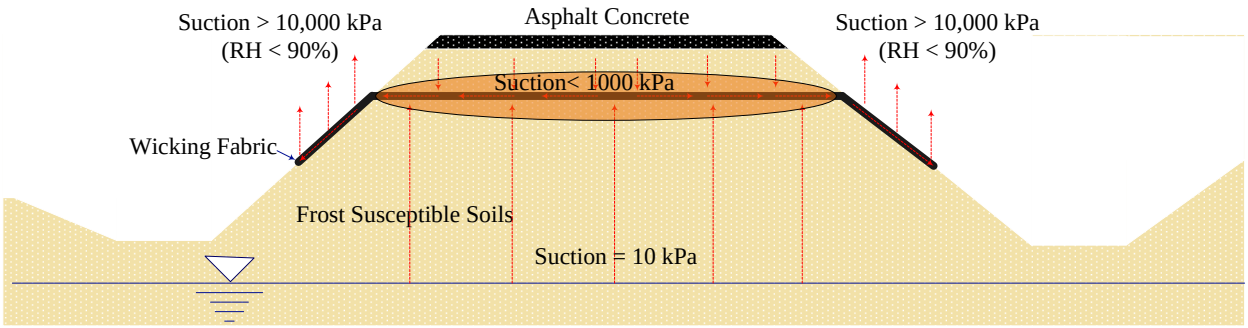

Figure 1.1 Working mechanism of H2Ri wicking fabric (original design)

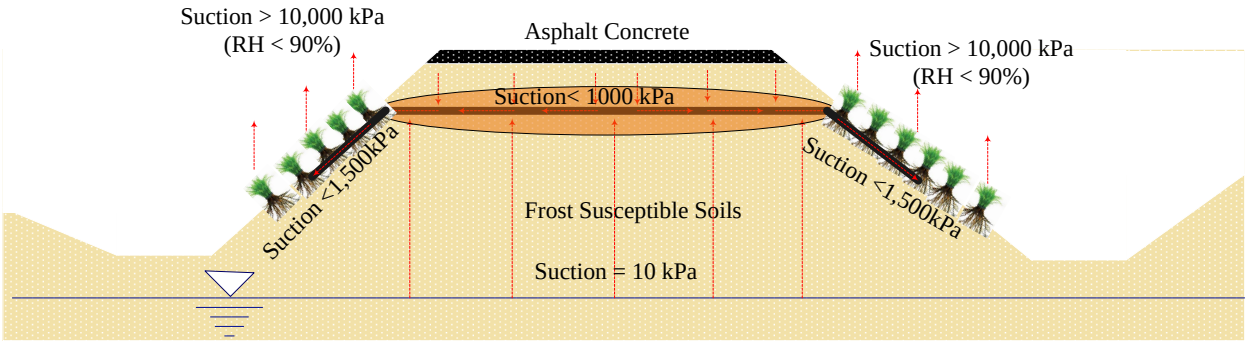

Figure 1.2 Working mechanism of H2Ri wicking fabric (revised design, proposed in this research)

1.2 Research Approach and Methodology

The objective of this research was to investigate the possibility of using a bio-wicking system that wicks water out of pavement structures. High moisture content within a pavement structure significantly reduces the resilient modulus and increases permanent deformation. By reducing the moisture content in the pavement structure, the long-term performance of the pavement can be improved. The objective was met through comprehensive study of the drainage efficiency of a bio-wicking system. The following tasks were accomplished:

Task 1: Literature Review

Task 1 involved a comprehensive literature search of published materials and ongoing research on suction and moisture measurements in vegetation root zones, soil-water

characteristics, unsaturated permeability and water transport rate for different soils, as well as dependence of resilient modulus and permanent deformations on moisture content and/or suction. Task 1 provided useful information on the wicking ability of H2Ri in different soils.

Task 2: Elemental Level Test for the Bio-Wicking System

Task 2 involved measuring moisture and suction response over time in the system (see Figure 1.3). The system was built, and vegetation was allowed to grow until it matured. Then soils in the box shown in Figure 1.3 were saturated, and the whole system was sealed with impermeable layers. The vegetation was allowed to grow in a controlled environment by wicking water out of the soils in the box with H2Ri. Temperature, soil moisture, and suction at three different locations of the system were measured during the testing period. No additional water was provided for the vegetation until it wilted due to lack of water from the box. The measured data were analyzed to evaluate the water transport rate at different suction gradients. This information was used to evaluate the bio-wicking system's drainage efficiency and compare it with the control case (no geotextile) and original (with geotextile exposed to the open air).

Task 3: Full-Scale Field Tests

Task 3 involved field test measurements of moisture and suction response in the system over time (see Figure 1.4). Unlike the soil box in Figure 1.3, the box in Figure 1.4 is much larger, with a length of 12 ft and a cross section of 1 ft by 1 ft. This measurement is used to simulate half of a two-lane road. A similar approach was used to build the testing flumes, and moisture distribution within the testing flumes was monitored. However, due to the longer length, it was expected that moisture and suction would not be the same at different locations. Moisture change and suction change along with time and locations were summarized into MATLAB videos to demonstrate the principle of water movement in the bio-wicking system. Measured moisture and

suction can be related to resilient modulus and permanent deformations to evaluate the benefit of the bio-wicking system. For comparison purposes, similar model boxes were built with no H2Ri wicking fabric; moisture response and suction response in the system over time were monitored.

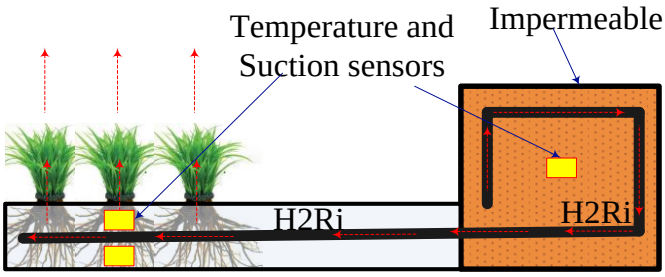

Figure 1.3 Design for the elemental soil test for the bio-wicking system

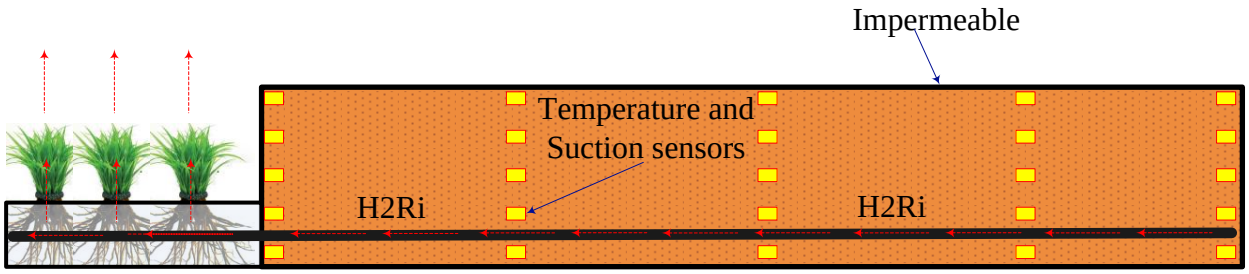

Figure 1.4 Model test for the proposed bio-wicking system

Task 4: Draft of Final Report and Recommendations

Task 4 involved the completion of a final report on Tasks 1 through 3. The results from those three tasks were synthesized and analyzed to provide recommendations on the bio-wicking system for improved road performance.

CHAPTER 2.0 LITERATURE REVIEW

The focus of this project was the development of a method to quantify and incorporate the benefits of H2Ri geotextile in dehydrating a road's base course, thus improving pavement system performance. In this chapter, the detrimental effects of water on pavement's long-term performance are discussed, the water sources in a pavement structure are examined, the applications of geosynthetics (especially geotextiles) in pavement structures are presented, and recent studies of bioengineering applications in civil engineering are demonstrated. General concepts regarding evapotranspiration processes are illustrated in detail to give a theoretical background regarding the proposed bio-wicking system.

2.1 Adverse Effect of Water in Pavement Structures

Since this project focuses on the application of a bio-wicking system in roadways, this section includes a discussion of the major disadvantages of traditional soil-geotextile systems in addressing moisture conditions in pavement structures. Most soil-geotextile systems aim to improve pavement performance by (1) enhancing lateral constraint, (2) increasing bearing capacity, and (3) reducing rutting issues by evenly spreading the wheel load. However, when comparing the thickness of a geotextile with the entire pavement structure, the reinforcement effect of a geotextile is limited. Potyondy et al. (2016) indicated that the resilient modulus could be doubled if the proper type of geogrid is adopted. Similarly, TenCate (2010) proved that the TBR (Traffic Benefit Ratio) value could be as high as 10, and the BCR (Base Course reduction Reduction) value could be 33% when pavement structure uses geotextile reinforcement material. However, Lin and Zhang (2016), who systematically studied an alternative method of improving pavement's overall performance by reducing the long-term water content of a pavement

structure, found that by reducing the water content of AB-3 base course from 8.5% to 6.5%, the resilient modulus increases by 3 times. A comprehensive review of the adverse effects of water on pavement structures follows.

Sources and Categories of Subsurface Water

Subsurface water exists in four forms: water vapor, bounded water, capillary water, and free (or gravitational) water (Kochina and Ya, 1952; Aravin and Numerov, 1953; Muskat, 1937). In most cases, water vapor is stored inside soil pores above the saturation zone. In existing subdrainage design methods, water vapor transmission is negligible. Bounded water is relatively hard to move from soil particles and can be considered part of soil particles. This part of the water phase in soil cannot move under gravity force and, therefore, is not considered in most subdrainage design methods. Capillary water also exists in soil pores above the saturation zone. However, unlike water vapor, capillary water flows under the action of surface tension. The height of capillary rise is a function of soil particle distribution, which relates to soil gradation curve and density (Lane and Washburn, 1946; Barber and Sawyer, 1952). Since capillary water cannot be drained by gravity, the most common way to control capillary water is to lower the water table or use a capillary barrier, which blocks upward capillary flow. The most common type of water, free water, is the water in liquid form that flows under the force of gravity and obeys Darcy's law. Controlling free water is the major concern in existing subsurface drainage design methods.

Subsurface water comes from a variety of sources and falls mainly into two categories: groundwater and infiltration. Groundwater refers to the water that exists in the saturation zone below the water table. Precipitation is the major source of groundwater. Infiltration water is defined as the water that seeps into the pavement structure through the pavement surface,

shoulder, or median. Precipitation is also the major source of infiltration water. For bituminous pavements, the primary infiltration water source is longitudinal joints at shoulders and construction joints between strips of paving. As for concrete slabs, infiltration water enters through cracks, joints, and shoulders (Cedergren, 1974; Cedergren et al., 1973).

Adverse Effects of Water in Pavement Structures

Excessive water in a pavement structure is recognized as one of the major adverse factors that influence pavement's overall performance. Excess water can cause a variety of engineering problems; for instance, it can cause soil expansion and collapse, reduce soil strength and stiffness, increase excess pore water pressure and develop seepage forces, strip asphalt pavement, and generate cracks (Han and Zhang, 2014). Both dynamic traffic load and thermal shrinkage induce cracks within the asphalt pavement layer. Cracks are partially or completely filled with water through infiltration, which results in saturation of base and subgrade materials over time. Higher pore water pressure is induced by large dynamic loading of heavy duty vehicles, causing free water within the base and subgrade, together with fines, to squeeze out of the pavement structure. This phenomenon is called pumping. Free water wedges are produced beneath the asphalt pavement. Wet softened areas due to loss of fines in the base and subgrade layers cause potholes or depressions of the pavement structure. Similar pumping phenomena also occur in Portland cement concrete (PCC) pavements (Mallela et al., 2000). Upward curl of pavement slabs (resulting from uneven temperatures above and beneath the cement pavement slab) tends to create small pores. Free water can easily penetrate and saturate base and subgrade layers via joints through precipitation and infiltration. Upcoming wheel load causes the backward slab edge to deflect downward and generates large pore water pressure. When the wheel passes the joint, the forward slab deflects downward and the previous backward slab

rebounds upward. The cyclic downward deflecting–upward rebounding process pumps water out of the pavement structure together with fines. The materials beneath the joints of slabs erode over time, and faults or cracks near the joint further accelerate the deterioration process.

Adverse Effects of Water in Cold Regions

Another adverse effect of water on pavement structure is called "frost boiling," which causes extensive damage in northern regions or cold climates. The mechanism of frost boiling phenomena is related to frost heave and thaw weakening processes (Chamberlain, 1987). In coarse-grained base, subbase, and subgrade courses, water drains out fast. However, when water encounters course material with more fines, it causes the fines to intrude into the base layer due to dynamic traffic load, and water migration causes differential settlement. Frost heave is attributed to the formation of ice lenses during freezing. Three key elements are required in ice lens formation: (1) frost-susceptible (FS) soils, (2) subfreezing temperatures, and (3) available water sources. Frost-susceptible soils are defined as soils with pore sizes between particles and particle surface area that promote capillary flow (Casagrande, 1947; Csathy and Townsend, 1962). For engineering practices, soils containing over 10% fines are considered FS soils. During the freezing period, water in a large void space freezes into ice crystals as the freezing front moves downward. Water expands about 9% by volume and is considered impermeable when frozen. Negative pore water pressure is generated, and ice crystals tend to attract water from adjacent voids. However, frozen soil above the freezing front is impermeable, and the only available water source comes from the unfrozen subgrade beneath the freezing plane. As crystals continue to grow and are fed by capillary movement through FS soils, shallow groundwater continuously flows upward to the freezing plane causing pavement to heave and sometimes crack. As the upcoming spring rises, the ice lens starts to melt and causes softened areas within

the pavement structure (Taber, 1930 a and b; Miller, 1978). When water drains out over time, differential settlement phenomena can be observed. Soft and weak soils provide limited friction and interlock between subgrade and base materials, resulting in rutting issues.

2.2 Geosynthetics Applications

Geosynthetics Category and General Applications

Geosynthetics are synthetic and polymeric materials used in civil engineering, and have eight major product categories: geotextiles, geogrids, geocells, geomembranes, geofibers, geofoams, geosynthetic clay liners, and geocomposites (see Figure 2.1).

Figure 2.1 Geosynthetics categories

Geosynthetic materials have two major applications: earth infrastructure reinforcement and erosion control, including slope protection and stabilization, building surface protection and decoration, road shoulder erosion control, and foundation reinforcement (Peng et al., 2000; Khing et al., 1993; Niroumand and Millona, 2010; Qian et al., 2013; and Han and Thakur, 2014). Geotextiles are continuous sheets of woven, nonwoven, knitted, or stitch-bonded fibers or yarns (Bathurst, 2007). Geogrids are uniformly distributed arrays of apertures between longitudinal and transverse elements (Muller and Saathoff, 2015). Geocells are relatively thick, three-dimensional networks constructed from strips of polymeric sheet. The interconnected cells are often filled with soils or concrete to enhance the stiffness of an infrastructure. Geosynthetic clay liners (GCL), geonets, geomembranes, and geocomposites are commonly used in environmental engineering protection projects. Geosynthetic clay liners are prefabricated geocomposites with a bentonite clay layer incorporated with two layers of geotextiles on the top and bottom, or bonded to a geomembrane; they can be used as a capillary barrier for contamination control and water dam hard-core protection. Geonets are open grid-like materials with polymeric strands at a constant acute angle. Due to large in-plane porosity, geonets are often designed as high drainable materials and applied with small drainage pipes or spacers. Geomembranes were originally designed for lining soil-waste landfills in the early 1980s; their primary function is as a liquid or vapor barrier or both. Geofoams are products created by a polymeric expansion process of polystyrene, resulting in a “foam” that consists of many closed but gas-filled cells. The skeletal nature of the cell walls is the unexpanded polymeric material. The resulting product is generally in the form of large, but extremely light blocks, which are stacked side-by-side, providing lightweight fill in numerous applications.

Geosynthetics have been used in the design of pavement to improve its performance. The major functions of geosynthetics are separation, confinement and reinforcement, filtration, and drainage. The improved performance of pavement due to geosynthetics reinforcement has been attributed to three mechanisms: (1) lateral restraint; (2) increased bearing capacity; and (3) tensioned membrane effect (Giroud and Noiray, 1981; Giroud et al. 1984; Perkins and Ismeik 1997 a and b; Holtz et al. 1998). Among the geosynthetics materials shown in Figure 2.1, geotextiles and geogrids are two types commonly used to treat pavement distress in flexible pavements. Geotextiles and geogrids can be used as separation materials; placed between the two dissimilar materials, they maintain the integrity of both materials. For confinement function, geotextiles and geogrids can be used to prevent aggregate lateral movement, which can compromise roadway and pavement structure performance (Bueno et al., 2005). Geotextiles take advantage of friction, while geogrids use interlock to mitigate relative movement. For reinforcement function, both geotextiles and geogrids work effectively to spread the load and prevent excess load on different components that make up the road (Benjamin et al., 2007). In addition, geotextiles are used beneath the asphalt overlay to mitigate crack propagation. Even though geotextiles and geogrids provide separation, confinement, and reinforcement, when it comes to filtration and drainage, geotextiles function better than geogrids. Geotextiles allow free water to flow across the geotextile plane while controlling soil particle retention. As water and small particles drain through confined layers of aggregate and subgrade, smaller particles eventually are trapped between bigger ones, resulting in larger grading and providing more stable layers. It is impossible to grade aggregates by using a geogrid because the product has much larger openings.

Geotextiles in Pavement System

Geotextiles have proved effective as drainage and/or moisture barrier layers when in contact with partially saturated soils (Henry, 1998; Stormont et al., 1997; Henry and Holtz, 1997; Stockton, 2001; Krisdani et al., 2008). As for use as a moisture barrier, Henry and Stormont (2002) first named and patented the capillary barrier as "geocomposite capillary barrier drain (GCBD)." A capillary barrier is composed of a layer of relatively low-permeability material over a more highly permeable material. In a pavement system, a capillary barrier is referred to as a high-conductivity material at the interface of the aggregate base course (ABC) and subgrade to divert infiltrated water laterally toward the edge drain and to minimize moisture variation in the profile (Christopher et al., 2000; Henry et al., 2002; Stormont et al., 2009).

The geotextile in a pavement structure is rarely saturated. The unsaturated property of the geotextile is a key design factor in determining the pavement's long-term performance. Typically, the water characteristic curve (WCC) for both soil and geotextile, and in-plane transmissivity are two important terminology depicting hydraulic behaviors. The WCC depicts the relationship between the water content of a porous material and the potential energy of the pore water. Two important parameters of the geotextile are critical to determine the geotextile drainage efficiency: air entry value (AEV) and water entry value (WEV). The AEV is defined as the suction value at which an initially saturated porous material begins to desaturate (related to the largest pore size in the matrix). The WEV is defined as the suction level at which water starts to enter the initially dried porous media. These two parameters allow the geotextile to function as both drainage and barrier material (Zornberg and Mitchell, 1994). When the suction value is lower than the air AEV, the porous material is considered saturated and exhibits saturated hydraulic properties. The hydraulic conductivity of the porous material significantly decreases

when the suction value surpasses the AEV. Under high suction range, the geotextile can function as a capillary barrier. However, as water accumulates near the capillary barrier, the moisture content of the soil adjacent to the geotextile gradually increases (and the suction value decreases). When the suction value is smaller than the geotextile WEV, the hydraulic conductivity of the geotextile increases dramatically and the geotextile functions as drainage material (Stormont et al., 2001).

2.3 Bioengineering Applications

Vegetation is increasingly being used in civil engineering to enhance environmental sustainability. Bioengineering is the use of living plants in combination with infrastructure to control soil erosion and provide reinforcement function. Vegetation acts as reinforcement in three ways: (1) roots provide anchorage, and absorb water and nutrients from the soil; (2) stems support the aboveground parts and capture eroding soil; and (3) leaves intercept precipitation and initiate evapotranspiration, leading to decreased soil moisture levels (Coppin and Richards, 1990). Grass is commonly used together with geosynthetics to form a bio-engineering system to protect slope facings, unpaved shoulders, and parking lots. Recent advancements in bioengineering technologies using geosynthetics products are discussed in this section.

Shoulders in paved and unpaved roads are designed for emergency parking and providing structural support for the roadway. Runoff from pavement to the shoulders often causes soil erosion. A number of researchers have studied the effectiveness of vegetation as a protective layer for water erosion control (Morgan and Rickson, 2003; Zheng, 2006; Loch, 2000). Coppin and Richards (1990) indicated that the shear strength of a root-stabilized slope depends on root density, tensile strength, tensile modulus, length/diameter ratio, surface roughness, alignment, and orientation. The reinforcement of a root-stabilized slope is demonstrated in Figure 2.2.

Considering the worst case, if the slope is saturated (under seepage condition), the system's factor of safety is composed of two parts: one part is the additional reinforcement fraction (the left term in Figure 2.2) that is provided by the grass root; the second part is the slope's intrinsic friction when saturated (the right term in Figure 2.2). The apparent cohesion of the root-stabilized soil, c_a, varies from 1 to 17.5 kPa, and the typical root depth varies from 0.3–1.2 m. Han and Guo (2015) indicated that for a specific system, the factor of safety is 1.65 with vegetation and 0.55 without vegetation. Therefore, vegetation cover is an effective way to increase slope stiffness.

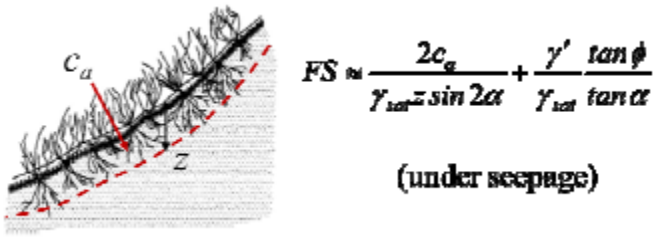

Figure 2.2 Root stabilization of surficial slope

Erosion is caused by water and by wind. In rural areas, road shoulders are often unpaved. Shoulders are also often buffeted by turbulent airflow induced by high-speed vehicles, resulting in dust emission (Moosmuller et al., 1998). Wind erosion causes up to 25% organic carbon and nitrogen loss, and jeopardizes vegetation survival (Li et al., 2007). However, if surface soil is covered with vegetation, wind velocity decreases within the space occupied by vibrating leaves, the soil beneath the vegetation is sheltered from erosional forces, and the rate of soil particle transport decreases to an allowable range.

A geosynthetics erosion control mat is a typical application of a combination of geosynthetics and vegetation. A permanent erosion control mat is often used for steep slope erosion control. A temporary erosion control mat is designed for road shoulders and flat slope protection before vegetation is established. Steep slopes are common in highway construction;

permanent erosion control is needed if the slope excavation angle is greater than 30° (Collin, 1996). Vegetation establishment is difficult on steep slopes because water cannot be retained. Morgan and Rickson (1995) proved that erosion control mats are effective at reducing rain splash during high-intensity rainfalls, thus reducing soil erosion.

Another common bioengineering application of geosynthetics is stabilization of unpaved shoulders and parking lots. Geocells are used to provide a firm surface for vehicular traffic. The geocell frame is porous and allows water to flow in all directions. Based on the specific design purpose, geocells are backfilled with different types of soil. For instance, if the road is designed only for constant vehicular traffic, or for parking without causing damage or rutting to grass, geocells are backfilled with topsoil. If the road is designed for withstanding very heavy vehicles, such as fire engines or semis, then geocells may be filled with aggregate. Finally, grass seed and fertilizer are applied to the surface. This bioengineering system using geocells produces a stiffer base and prevents lateral displacement of infill materials, which reduces rutting. This system allows for reduction in overall base thickness and enables subgrade materials to withstand more than 10 times the number of cyclic load applications, without the appearance of deflection that occurs in unconfined, unpaved roads. In addition, the system allows for the use of lower quality infill materials in situations where quality aggregates are not readily available, and helps with construction on soft soil subgrades.

2.4 Proposed Bio-Wicking System (Modified Design)

As noted in Chapter 1.0, the proposed bio-wicking system is another bioengineering application. In a previous project report (Lin and Zhang, 2016), the working mechanism of the soil-geotextile system and its efficiency at draining water from pavement structure were systematically discussed. With this advanced bio-wicking system, a layer of vegetation is applied

on top of the geotextile, which is extended to the road slopes. The field test at Beaver Slide proved its efficiency. The aims of the vegetation layer are to (1) reduce sunlight exposure and ultraviolet deterioration; (2) minimize the clogging effect and maintain geotextile drainage efficiency; and (3) ensure suction value lower than grass wilting point. The following is a discussion of the system's basic concept and previous research on evapotranspiration. An explanation of how the process of evapotranspiration influences the bio-wicking system's drainage efficiency is included.

Evaporation and Transpiration

Evaporation is a major component of the water balance of local, regional, and global systems (McMahon et al., 2013). Baumgater and Reichel (1975) reported that evapotranspiration composes approximately 70% of precipitation. Therefore, it is critical to review the historical development of evapotranspiration estimation. Evaporation is defined as the summation of all processes in which liquid water is transferred as water vapor to the atmosphere. Monteith (1991) indicated that three major factors affect the rate of evaporation from a wet surface: (1) the physical state of ambient air, (2) the net available heat, and (3) the wetness of the evaporating surface. Two processes influence the exchange of water molecules between the water surface and air: condensation and vaporization. Condensation is the process of capturing water molecules escaping from surface water, and vaporization is the movement of water molecules away from surface water. The difference between vaporization rate and condensation rate is defined as evaporation rate (Shuttleworth, 1992). For evaporation to occur, energy is used both for obtaining vaporization latent heat and for removing water vapor from the evaporation surface. According to Penman (1948), the main resistance to evaporation flux occurs within a thin nonturbulent layer of air (1–3 mm) next to the water surface. This resistance is defined as

aerodynamic or atmospheric resistance. In addition, there is little consistency in the units for input data. Generally, evaporation can be expressed in two units: depth per unit time ($mm \cdot day^{-1}$) or available energy per unit time ($MJ \cdot m^{-2} \cdot day^{-1}$). Because the latent heat of water at 20°C is 2.45 $MJ \cdot kg^{-1}$, 1 $mm \cdot day^{-1}$ of evaporation equals 2.45 $MJ \cdot m^{-2} \cdot day^{-1}$.

On the other hand, transpiration represents the evaporation from within the leaves of a plant via water vapor flux through leaf stomata (Dingman, 1992). The transpiration process can be estimated using the combination of Penman (1948) and Penman-Monteith (Monteith, 1965) equations. Net incoming solar radiation is the major energy source so that water advection and heat storage during the transpiration process are neglected. Moreover, ground conduction is ignored due to the vegetation coverage on the ground surface. The major resistance affecting transpiration is surface resistance, which depends on the degree of stomatal opening in the leaves and regulates the transpiration process (Monteith, 1991). Evapotranspiration is the sum of evaporation and transpiration from the soil surface (Allen et al., 1998).

CHAPTER 3.0 TEST DESIGN AND CONSTRUCTION PROCESS

3.1 Soil and Grass Properties

Soil Properties

The gradation curve for E-1 material is shown in Figure 3.1. The tested soil was a well-graded gravel with sand; the soil contained about 14.5% fines. This soil is classified as A-1-a according to AASHTO classification, or well-graded gravel with silt and sand (GW-GM). This type of soil is typical of soil used in an airport surface course in Alaska. In order to support heavy aircraft load, the soil needs to be dense-graded; hydraulic conductivity is expected to be small.

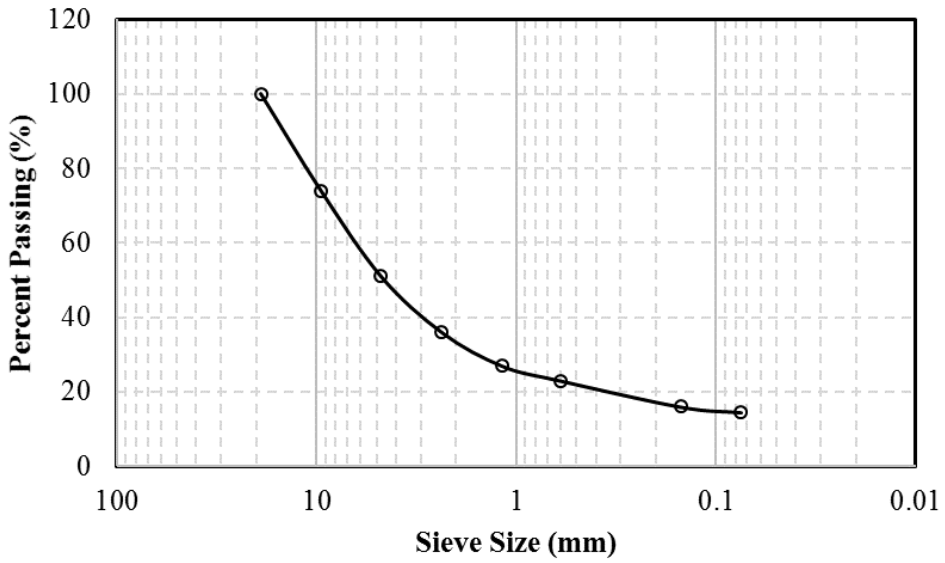

Figure 3.1 Gradation curve of tested E-1

As discussed in Chapter 2.0, the soil-water characteristic curve (SWCC) of a soil is important in analyzing soil hydraulic conductivity. An EC-5 moisture sensor was used to record volumetric moisture content variations within the testing boxes and flumes. In order to determine

the relationship between volumetric water content and gravitational water content, the testing method shown in Figure 3.2(a) was proposed. The sensors used consisted of an EC-5 moisture sensor for determining volumetric water content and a water potential sensor for determining suction value at the same time. The mass of the glass jar and sensors was measured first; then the soil was backfilled into the glass jar. Finally, the glass jar with sensors was wrapped with a plastic sheet to prevent moisture loss. The glass jar was exposed to open air for 10–15 minutes every day to reduce moisture content. During the rest of the testing period, the glass jar was kept sealed to ensure that equilibrium was achieved before the next measurement. The total mass of the glass jar containing soil was measured each time, and the glass jar was oven-dried after the test was accomplished. The gravitational moisture content could be determined from each measurement, and the corresponding suction value was obtained from the water potential sensor. The relationship between volumetric and gravitational moisture content is shown in Figure 3.3(a). For suction values greater than 1000 kPa, this testing method would take too long for each testing point; therefore a salt concentration test was used to determine the SWCC for suction values greater than 1000 kPa, as shown in Figure 3.2(b). The samples were put into containers made of tinfoil, and the bottom of each container was punched with small holes to shorten the waiting time for obtaining equilibrium. The osmotic suctions of different electrolyte solutions were adopted to calibrate the relationship between suction and soil moisture. The $MgCl_2$ concentration table is shown in Table 3.1. The samples were put into the desiccator for 7 days before measuring the water content of the samples.

(a) SWCC testing equipment (suction < 1000 kPa)

(b) Concentration test (suction > 1000 kPa)

Figure 3.2 SWCC test equipment

Table 3.1 Salt concentrations and corresponding suction

Solute No.	**$MgCl_2$ (g/L)**	**Suction (kPa)**
1	19.050	1303
2	38.100	2739
3	47.626	3523
4	66.676	5244
5	95.251	8249
6	142.877	14554

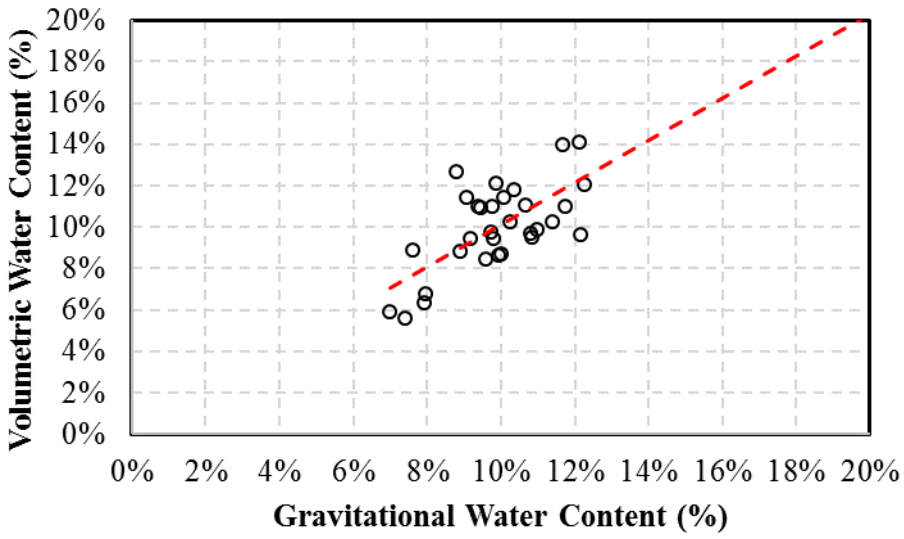

(a) Sensor calibration

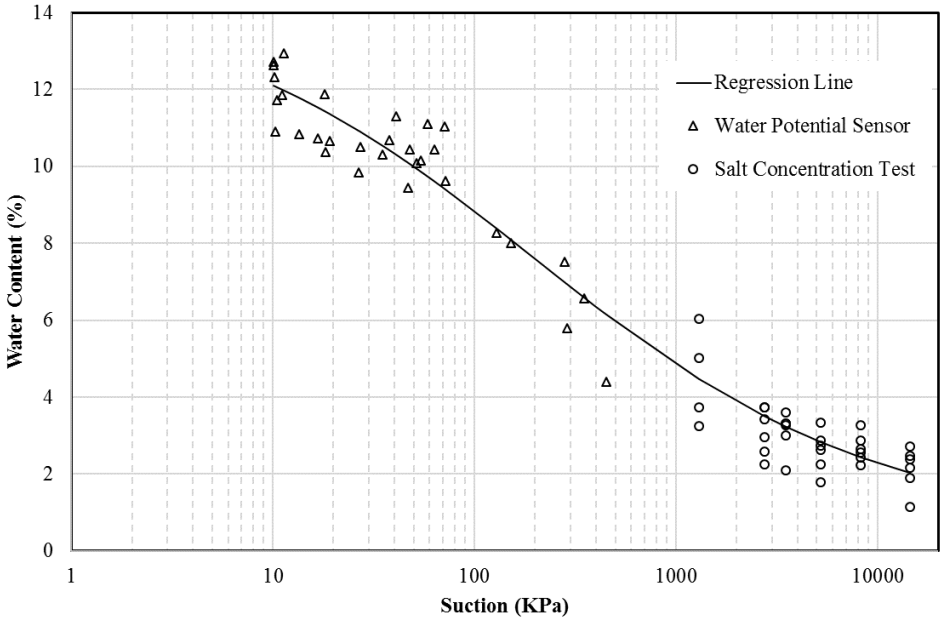

(b) SWCC plot

Figure 3.3 SWCC test method

The SWCC is presented in Figure 3.3(b). Because the monitoring range for water potential sensors was relatively large (10–9999 kPa), the sensors had difficulty measuring suction values smaller than 10 kPa. Based on the test results, the SWCC for E-1 material could be regressed as:

$$w = 0.143\left[\frac{1}{ln\left[2.718+\left(\frac{s}{131.9}\right)^{0.515}\right]}\right]^{2.027} \quad 3.1$$

where *w* is gravitational water content, and *s* is corresponding suction value.

Grass Properties

The Alaska Department of Natural Resources has published a manual, entitled "A Revegetation Manual for Alaska" (Wright, 2008). This manual, which serves as a guideline for revegetation projects in Alaska, comprehensively introduces the types of seeds currently used in Alaska, how to properly select the seed blend, what type of fertilizer to use, and how to select suitable equipment. The manual recommends a seed blend based on state regions (arctic, interior, western, southwest, south central, and southeast), soil moisture conditions (hydric, mesic, and xeric), and soil types according to engineering classification. The authors selected the seed blend according to recommendations from the Alaska Department of Transportation and Public Facilities (ADOT&PF): 60% nortran tufted hairgrass, 30% arctared red fescue, and 10% annual ryegrass. Figure 3.4 shows an image of the vegetation produced by each seed.

(a) Nortran Tufted Hairgrass (b) Arctared Red Fescue (c) Annual Ryegrass

Figure 3.4 Selected seed blend

Nortran tufted hairgrass was released by the University of Alaska Agricultural Experiment Station in 1981 as a forage and revegetation grass in northern areas. This cultivar has proved better adapted to northern regions of Alaska. Arctared red fescue is outstanding for erosion control and good for preventing the invasion of native shrub species such as alder and willow. However, this seed is unacceptable in reclamation due to its overly aggressive, sod-forming nature. Annual ryegrass provides a quick, temporary cover and should be limited to 10% or less of a seed blend. The use of these species should be limited because the plants use nutrients that are intended for the perennial species in the mix and produce a heavy cover, slowing the growth of the perennial species. Annual and perennial ryegrasses are also very attractive to herbivores, causing potential vehicle/animal conflicts.

3.2 Elemental Level Box Test

Test Design

The elemental level box test includes three testing boxes: S1, S2, and S3. Test box S1 is shown in Figure 3.5(a). This test box represents the control case, without geotextile or grass. The test box dimensions are 36 in. (L) × 16 in. (W) × 16 in. (H). The entire test box was covered with a double layer of 6 mil plastic wrap to prevent water from leaking from the system. The test box was filled with E-1 material to a height of 12 in., and two layers of sensors were buried at depths of 1.5 in. and 6 in. from the bottom of the test box. In the horizontal direction, each sensor was located 6 in. from the edge of the test box. Two types of sensors were adopted at each location: one was an EC-5 soil moisture sensor, and the other, an MPS-2 dielectric water potential sensor (measuring suction). To be consistent with the other two test boxes, S1 had several pre-drilled drainage holes at the left bottom corner to allow excess water to flow out of the testing system.

The test design for S2 is show in Figure 3.5(b). This test box was used to simulate the conventional application of the geotextile. Test boxes S1 and S2 had the same test design inside the box except that for S2, a layer of geotextile was located at a depth of 1.5 in. from the bottom and had a 4 ft extension outside the test box. This time, the test box was precut with an opening of 13 in. (W) × 0.5 in. (H) for the geotextile to pass through. Outside the test box, the geotextile was sandwiched by E-1 material (1.5 in. beneath and 2 in. above). An extra pair of sensors was located 2 ft from the tail end of the geotextile and 1.5 in. above the ground. In contrast, test box S3 was aimed at simulating the bio-wicking system to wick water out of the testing system. The test designs for S2 and S3 were the same, except that the geotextile in S3 was covered by a layer of 3.5 in. thick blended soil, rather than the E-1 material used in S2.

By analyzing test box S1, the natural drainage efficiency of the testing system could be determined. Under this condition, only free water drained out of the system; the capillary water was considered undrainable. By comparing S1 and S2, geotextile drainage efficiency could be quantified. The moisture differences for S1 and S2 at the same location indicated how much excess water (mostly capillary water) was drained out by using a layer of geotextile. Moreover, comparisons of S2 and S3 indicated drainage efficiency by only considering the evaporation process (S2) or considering both evaporation and transpiration processes (S3). By comparing systems, the authors could quantify the benefit(s) of a bio-wicking system, only adopting the geotextile. Finally, the overall improvement of the bio-wicking system drainage efficiency could be analyzed by the comparisons of S1 and S3.

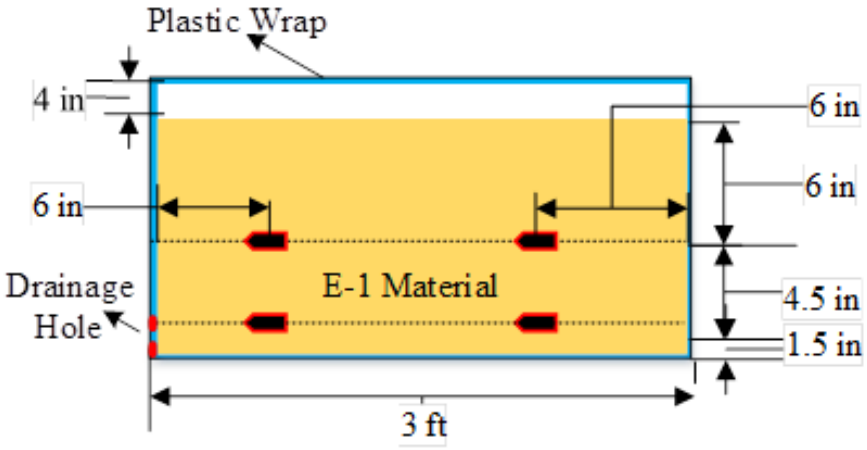

(a) Test Box 1, no geotextile, no grass (S1)

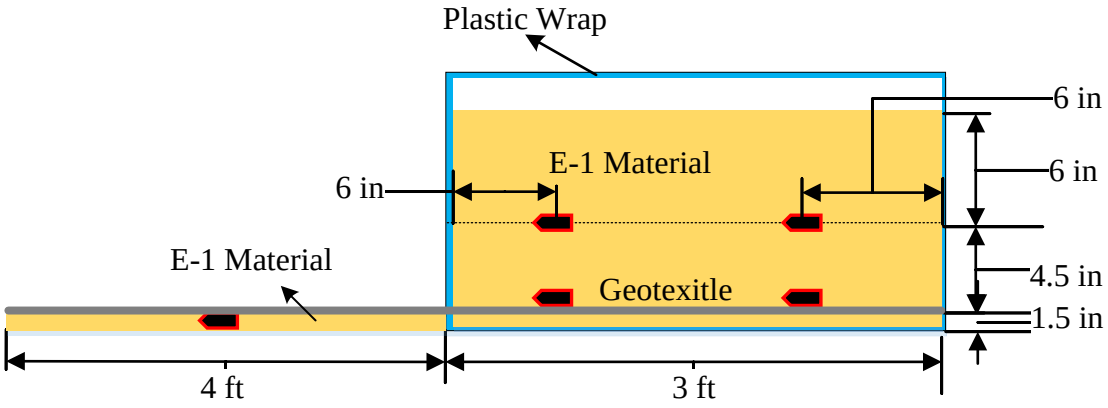

(b) Test Box 2, with geotextile, no grass

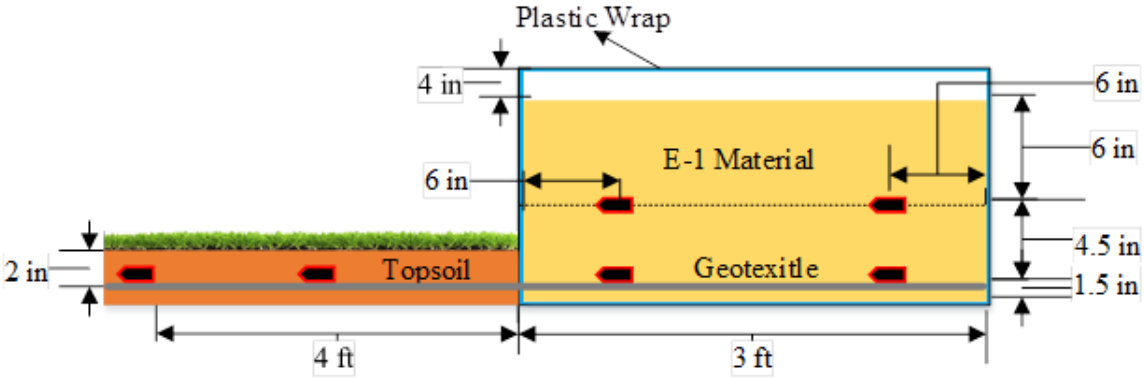

(c) Test Box 3, with geotextile, with grass (S3)

Figure 3.5 Schematic plot of elemental level test boxes

Construction Process

The test box construction process is shown in Figure 3.6. Since the test boxes are made of plastic, they have the potential to split under the heavy weight of soil. To prevent the test box from expanding or splitting, two horizontal wood beams were added to increase stiffness. The top of the test box was equipped with a wooden holder to support the horizontal beam. The sidewall of the plastic box was first cut to a 2 in. (W) × 0.5 in. (H) joint to fasten the horizontal beam. Then, the sidewall of the test box was squeezed and screwed together with a wood stud and plywood, as shown in Figure 3.6(a). Next, the testing box was covered with a layer of 6 mil plastic wrap. Due to the irregular box shape, the plastic wrap had to be folded at the corners to ensure maximum box capacity. The plastic wrap was at least 2.5 times longer than the box length and 5 times wider than the box width so that the extra plastic sheet could be used to cover the top of the soil entirely and prevent water from infiltrating the system.

(a) Test box supporting base (b) Test box horizontal beams

Figure 3.6 Test box construction

After the beams had been made, the drainage holes and the opening (for the geotextile to pass through) were drilled and cut, as shown in Figure 3.7(a). Extra attention was necessary in cutting the opening because the test box was relatively brittle. Beneath the opening, a row of drainage holes allowed excess water to drain out of the system. The opening for the geotextile was subject to closure due to the heavy overburden of soil. Closure of the opening would have impeded the drainage efficiency of the geotextile or even cut off the geotextile, so two wood beams were used at the sidewall of the test box to provide additional support.

(a) Geotextile opening and drainage holes (b) Wood stud support

Figure 3.7 Test box supporting system

After the test boxes were in place, E-1 material was backfilled and the sensors were installed, as shown in Figure 3.8(a). Since the E-1 material was stored in buckets near the testing site, extra care was required to ensure that the soil was well blended before putting it into the test box. The soil was evenly spread and leveled before the sensors were put into the target locations. For test boxes S2 and S3, a layer of geotextile was installed at a depth of 1.5 in., as shown in Figure 3.8(b). The sensors were directly in contact with the geotextile, and one shovel of E-1 material was gently piled on the sensors to keep them from moving around. Then extra E-1 material was carefully filled to a height of 4.5 in. (the target height to install the next layer of sensors).

(a) Sensor installation (b) Geotextile installation

Figure 3.8 Soil backfill and sensor installation

The next step was to install the sensors outside the test box, as shown in Figure 3.9. A layer of blended soil 1.5 in. thick was first spread on the ground and compacted. Two pairs of sensors were installed 2 ft and 4 ft from the test box. Then the geotextile was laid on top of the sensor followed by another 2 in. of blended soil. Next, the blended soil surface was raked with a fan rake, and the grass seed was gently applied. Finally, the soil was watered lightly and kept moist so that the seed could germinate and the vegetation could become established.

(a) Sensor installation (b) Soil compaction (c) Seed application

Figure 3.9 Sensor installation and grass seed revegetation

3.3 Field Section Construction

Test Design

The aim of the test design was to simulate the drainage efficiency of half of a two-lane roadway installed with a bio-wicking system. As with the elemental level test boxes, the authors wanted to quantify drainage efficiency improvement by comparing the bio-wicking system that had a vegetated surface, with a conventional geotextile system in which geotextile was exposed to the air, and with geotextile sandwiched between E-1 material.

Figure 3.10(a) shows the test design of the field section. In total, ten testing flumes were built. The revegetation area was 9 ft (L) × 8 ft (W) in size. Eight out of the ten geotextile strips were buried in the revegetation area. Four geotextile strips on the left side were buried at a depth

of 1 in.; the other four were buried at a depth of 2 in. Each testing flume was 12 ft in length; the space between two flumes was approximately 0.5 ft. Each testing flume had an area 9 ft long with geotextile (close to the vegetation area) and an area 3 ft long without geotextile. In addition to geotextile buried under grass, two other types of installation method were used: with geotextile directly exposed to the open air (Testing Flume 10, hereafter referred to as T10), and with geotextile buried under E-1 material (T5).

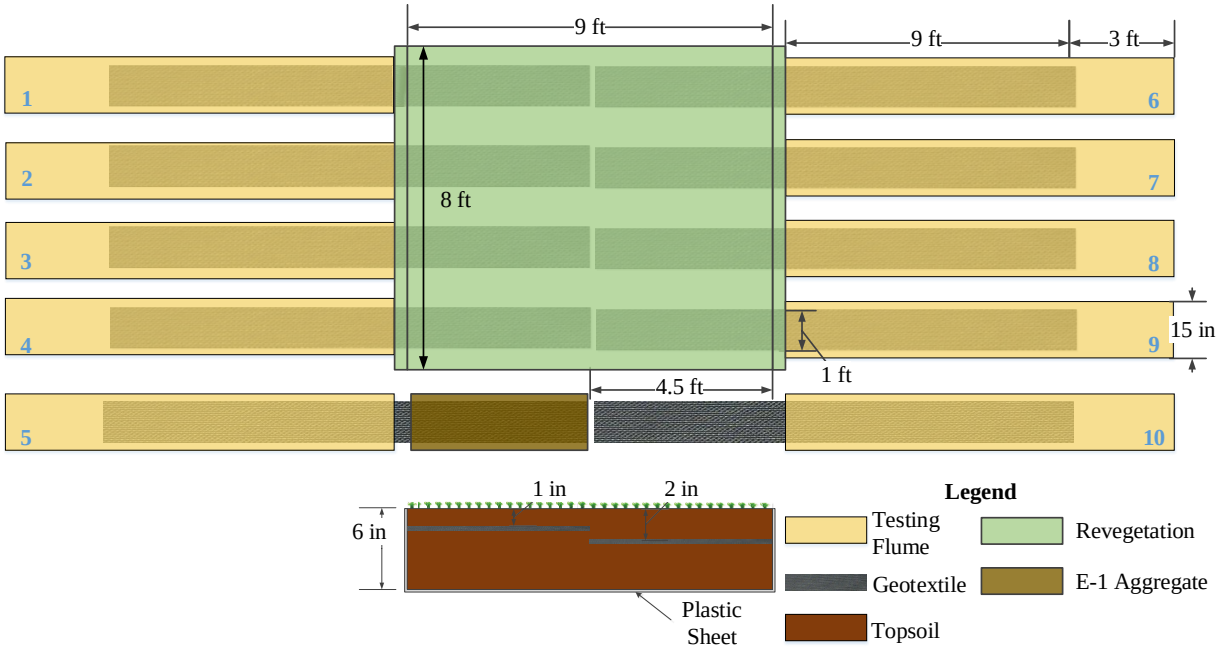

(a) Top view

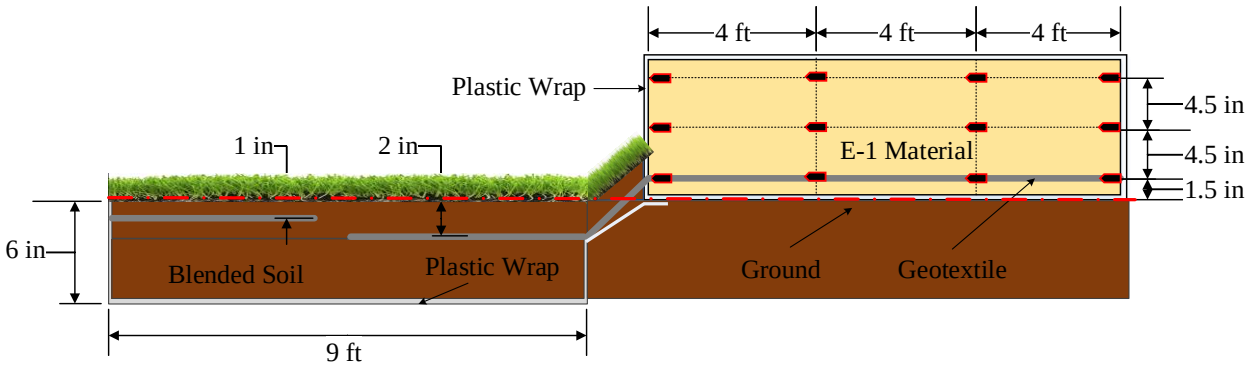

(b) Front view

Figure 3.10 Field test design

Figure 3.10(b) gives the front view of the bio-wicking test system. The testing flume sat on the ground with 3 layers containing 12 sensors located at depths of 1.5 in., 6 in., and 10.5 in. from the bottom of the testing flume. In each layer, the sensors were spaced 4 ft apart. The geotextile was installed at a depth of 1.5 in. from the bottom. The testing flume was covered with plastic wrap to prevent external water from infiltrating the system. The revegetation section was 6 in. in depth and surrounded with plastic wrap. The geotextile was buried 2 in. from the ground surface. To prevent direct exposure of the geotextile to the air, the gap between the revegetation and testing flume was connected with a vegetated, smooth slope.

Figure 3.11 shows the schematic plot of the testing flume design. The base of the testing flume was composed of a 1.25 ft (W) × 12 ft (L) × 0.75 ft (H) plywood board. Because the overburden soil weight was heavy, the base was supported by a wood stud frame (Figure 3.11a). Figure 3.12 shows the front view of the testing flume. Four vertical wood studs were screwed into the plywood to frame one of the sidewalls of the testing flume.

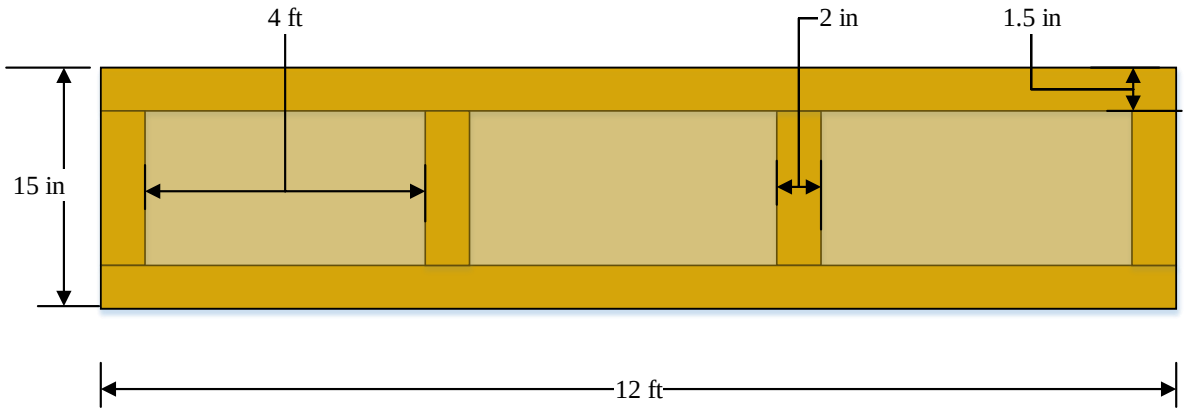

(a) Top view

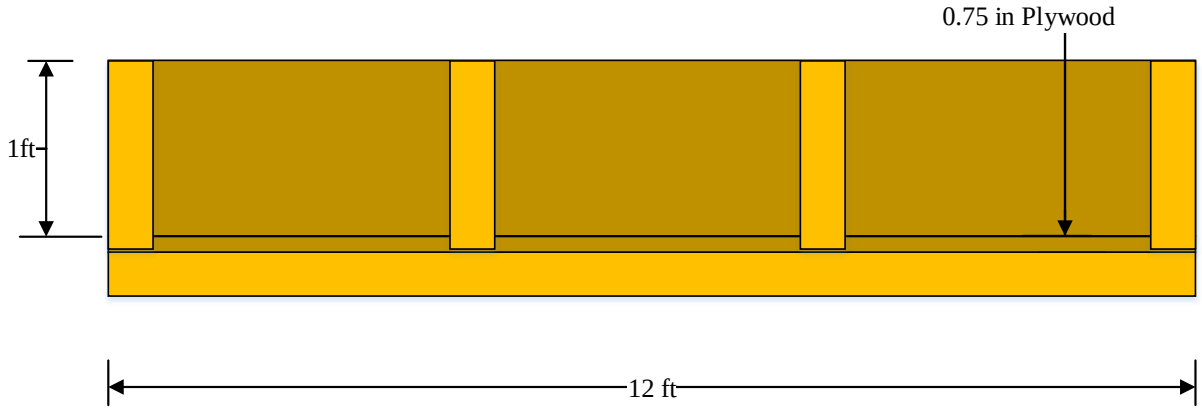

(b) Front view

Figure 3.11 Testing flume design

Grass Revegetation

The first step in developing the bio-wicking system design involved grass revegetation. First, the revegetation area (green color in Figure 3.10) was built. To control the ambient environment and evaluate the amount of water wicked out of the soil, a layer of 6 mil plastic wrap was implemented beneath and around the testing section to prevent external water from infiltrating the testing section. The soil refilling and compaction process is shown in Figure 3.12. The test section was cleared and excavated to a depth of 6 in., and the surface was leveled (Figure 3.12a). Then the top soil was mixed with the original soil at a ratio of 1:2. A lawn roller

weighted with water was used to compact and level the blended soil (Figure 3.12b and c). Before filling with another layer of soil, the surface of the compacted soil was evened out in four or five directions and raked with a fan rake to ensure good contact between layers of soil (Figure 3.12d).

(a) Test site clearance

(b) Plastic wrap installation

(c) Soil compaction

(d) Soil raking

Figure 3.12 Soil filling and compaction

Figure 3.13 shows the geotextile implementation procedures. After the soil was compacted to the targeted height, eight pieces of geotextile were put into the test section and fixed with cap nails (Figure 3.13a–b). Then the exposed geotextile strips were rolled together and covered with plastic bags. Next, half of the test section (lower section) was filled and compacted with blended soil; the same procedure was used in the other half. Care was taken to ensure that no geotextiles were in contact with each other to prevent interruption during the test. Because

each bio-wicking system was considered a separate system, overlapping of the geotextile might result in invalid test data.

(a) Wicking fabric layout

(b) Wicking fabric installation

(c) Soil compaction

(d) Soil raking

Figure 3.13 Wicking fabric installation process

After geotextile strips were implemented and the soil was compacted to the targeted height of 6 in., the surface was raked again to create shallow grooves for the seed to set, as shown in Figure 3.14. The grass seed and the fertilizer were evenly applied via a hand spreader. Then a thin layer of wood mulch covered the entire testing section to maintain the grass seed in moist condition during the germination and maturing process. The final step was to preserve the

geotextile strips, as shown in Figure 3.15. Two 1 ft (W) × 0.5 ft (H) ditches were excavated to bury the geotextile rolls in the ground (Figure 3.15a and b). Then the sheet of plastic wrap was placed at the bottom of the ditch, and the geotextile strips were wrapped with the plastic wrap (Figure 3.15c). The soil was backfilled to the ditch and compacted to the same level of the testing section (Figure 3.15d).

Figure 3.14 Grass seed revegetation

(a) Ditch excavation

(b) Geotextile in ditch

(c) Geotextile preservation

(d) Soil backfilling

Figure 3.15 Wicking fabric preservation

The grass revegetation was finished on July 11, 2015. Since no time remained to perform the test, the authors decided to postpone the test till July 2016. Figure 3.16(a) shows the appearance of the revegetation area after the snow had melted. Because the test section was thoroughly protected from water infiltration and runoff, the grass roots were dead due to the flooding of melting snow. Because it is essential to ensure that excess water can drain from the testing system, an additional ditch was built on the west side of the test section (see Figure 3.16b). The plastic wrap at the west edge of the test section was dug out. Then the plastic wrap was folded and buried at the bottom of the ditch so that excess water could drain. Finally, the ditch was backfilled with soil and leveled out to the same height as the test section.

Figure 3.16 Additional drainage ditch construction

Testing Flume Construction

The next step after construction of the revegetation area was finished involved building up the testing flumes and backfilling the E-1 material. The components of the testing flume were prefabricated, sent to the construction site, and assembled. After the testing flumes were finished, they were placed in location as discussed in the *Test Design* section (see Figure 3.17a). On each side of the test section, four testing flumes faced the previously buried geotextile strips and one was seated outside the test section. After the testing flumes were located at the target locations, two layers of 6 mil plastic were covered within the testing flume, as shown in Figure 3.17(b). One side of the plastic wrap was designed 3 ft longer so that it could serve as a cover on the testing flume to prevent water infiltration. Four horizontal beams were used to fix the plastic wrap in position and provide additional confinement.

Figure 3.17 Testing flume layout

After the testing flumes were ready, the geotextile rolls were dug out and cleaned with tap water, as shown in Figure 3.18(a). The purpose of washing the geotextiles was to clear out any organic debris or soil that remained on the surface. The geotextile rolls were then recovered with plastic bags before installation and temporarily put on the test section. The plastic wrap that had been used previously to preserve the geotextile rolls was laid out under the testing flumes. Using this method, the water that was wicked out by the geotextile would flow entirely to the revegetation area, and no water would run out of the system. Figure 3.18(b) shows the gap between the testing flume and the revegetation area. Because the relative humidity was very high (corresponding to a high suction level), the hydraulic conductivity of the geotextile was significantly decreased when suction was higher than its air entry value. In order to maximize geotextile drainage efficiency, the geotextile should not be directly exposed to the open air. Therefore, this 0.5 ft width gap also needed to be revegetated. In addition, the geotextile buried in the ground was about 7–8 in. lower than the geotextile in the testing flume. It is critical to ensure that the geotextile within the gap area has a gradual elevation increment. That is, the slope of the gap should not be too steep. Thus, the bottom of the geotextile was first gradually filled

with blended soil to the same elevation as the ground (see Figure 3.18b). Figure 3.18(c) shows the 0.5 in. opening that connected the geotextile with the revegetation area. The lower part of the sidewall was 1.5 in., which was the same as the geotextile installation height. In order to be consistent with the revegetation area, the geotextile surface was covered with a 2 in. layer of blended soil, and the soil extended to the opening where the geotextile passed through the testing flume. After that, the top of the soil was raked with a fan rake, and grass seed was evenly spread (see Figure 3.19d). Since daily sunshine hours for June in Alaska last over 20 hours and the highest ground surface temperature can reach more than 40°C, the evaporation rate is very high during daytime. It was necessary to spread a layer of mulch to keep the soil moist as the seed germinated and became established. The gap revegetation after construction can be seen in Figure 3.19(e).

(a) Geotextile rolls cleaning

(b) Gap between testing flume and revegetation area

(c) Half-inch opening for testing flume side wall

(c) Gap revegetation

(d) Gap revegetation with mulch

Figure 3.18 Gap revegetation process

E-1 Material Backfilling Process

Before the backfilling process started, the sensors were labeled and attached to the side wall, as shown in Figure 3.19(a). Four vertical wood strips were screwed onto the horizontal beam as indications of the height of the backfilled E-1 material. On each strip, the installation heights of the sensors were already labeled with a marker. Beneath each horizontal beam, there were three EC-5 soil moisture sensors. After the first 1.5 in. of E-1 material was added and loosely compacted, the geotextile strip was spread out in the testing flume. Then the first layer of sensors was installed, and one shovel of E-1 material was gently piled on top of each sensor to

secure it in the targeted position (see Figure 3.19b). As indicated in the test design, there is a 3 ft long section without geotextile installed. Figure 3.19(c) indicates that the spacing from the edge of the testing flume to the end of the geotextile was exactly 3 ft. The geotextile had been folded and buried in the ground for nearly a year, and the wrinkles along the folded area might have shortened the geotextile's physical length, without stretching out. During the geotextile installation process, the geotextile needed to be stretched for 10–15 minutes before putting it into the testing flume. Enough E-1 material should be available at the tail end of the geotextile to ensure that spacing is exactly 3 ft from the edge of the testing flume. After the backfilling process was finished, the top of the testing flume was covered with plastic wrap to prevent water infiltration, as shown in Figure 3.19(d). Small wood strips were screwed at the sidewall of the testing flume to seal the system from blowing wind.

(a) Testing flume with sensors

(b) Geotextile installation

(c) 3 ft spacing to the edge of the testing flume

(d) Testing flume after construction

Figure 3.19 E-1 Material backfill process

CHAPTER 4.0 TEST RESULTS AND DATA ANALYSIS

This chapter demonstrates the geotextile drainage efficiency by comparing moisture content distribution from the testing boxes and flumes. The general climatic data during the testing period are introduced, the test results of the elemental level boxes are discussed, and comparisons of geotextile drainage efficiency are presented. The test results of the field full-scale testing flumes are demonstrated, and the drainage efficiency of the geotextile under different conditions (exposed to air, buried under revegetation) are summarized. Finally, the mechanism of the bio-wicking system to wick capillary water is discussed and demonstrated.

4.1 General Climatic Data

Since the geotextile working mechanism is closely related to air suction value (which is a function of relative humidity, temperature, and precipitation), general climatic data are presented in Figure 4.1. Figure 4.1(a) shows daily precipitation data from June 15, 2016, to October 2, 2016. The figure indicates that both the frequency and intensity of rainfall were higher in July than in other months. Among 18 rainfall events in July, 12 reached a precipitation height of 0.2 in. Precipitation data will be used later in this chapter to explain moisture content variation in the vegetation area and its influence on geotextile drainage efficiency.

Figure 4.1(b) shows daily maximum, minimum, and mean temperatures during the testing period. The figure shows only the general decreasing trend in temperature, not temperature variations within a single day. When the precipitation figures are combined, it is apparent that deviations between maximum (or minimum) and mean temperatures decreased when heavy rainfall occurred during that day. The maximum temperature was on July 13 (31°C), and the

minimum temperature was below zero after September 23, 2016. If the temperature was lower than 0°C, the recorded data during that time should be unfrozen water content.

In further unveiling the relationship between temperature and precipitation data, Figure 4.1(c) shows the hourly temperature data obtained from the CR1000 datalogger. The daily temperature variation was as high as 30°C during sunny days and decreased to less than 10°C during rainy days. Moreover, since the datalogger was covered in a transparent plastic box and directly exposed to sunlight, the maximum temperature was higher than that shown in Figure 4.1(b).

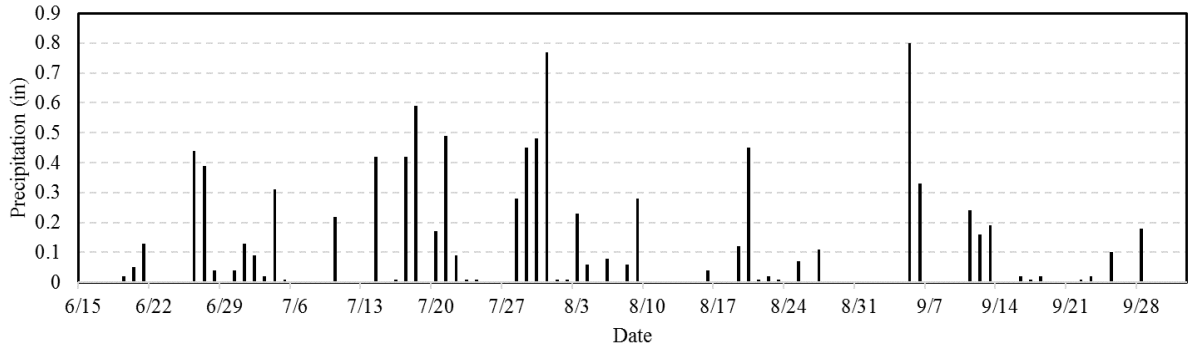

(a) Daily precipitation data

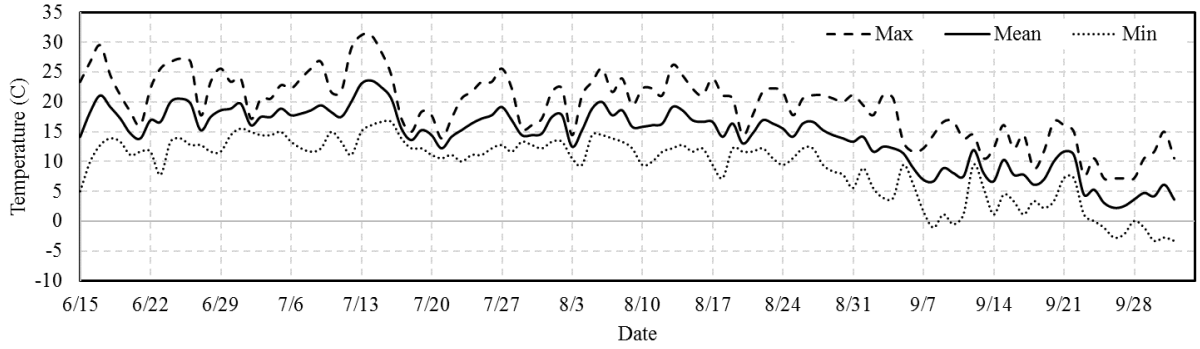

(b) Daily precipitation data

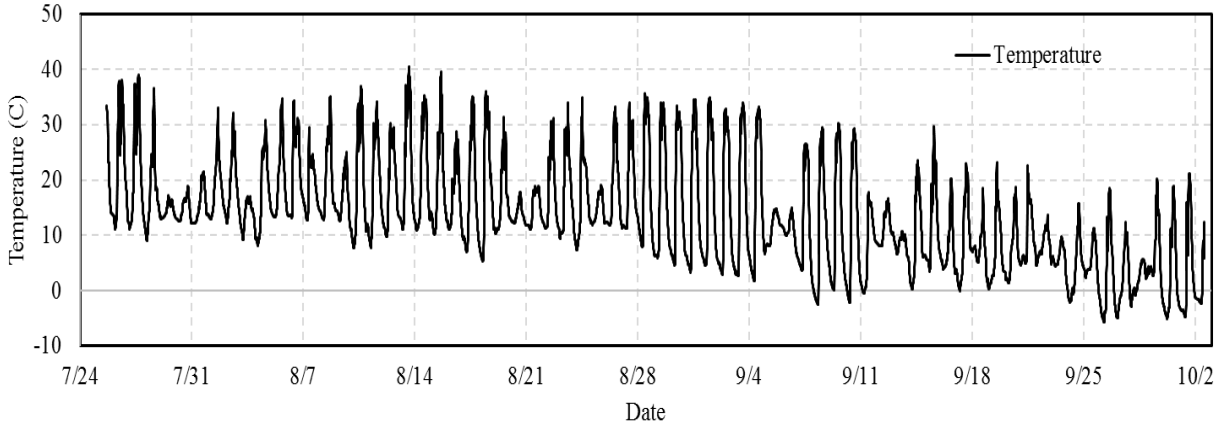

(c) Hourly temperature data

Figure 4.1 General climatic data

4.2 Elemental Level Test Results

The construction process for the small-scale testing boxes was completed on June 25, 2016, and the test was not started until July 13, 2016. Before the test started, the geotextile had already been working for 18 days, and all the testing boxes were saturated. In the following section, the moisture contours for different testing boxes at different testing stages are presented. Then a summary of the total volume of water within the testing flumes is demonstrated to compare the drainage efficiency of the bio-wicking system. In the figures, the contours for each moisture contour plot only show the area covered by four sensors and can only be used as an indication of the moisture condition within each testing box. The overall volumetric water content varied between 0 and 0.3, except for during the saturation period, when the moisture content could have been as high as 0.45. Therefore, the scale chosen for the color map is 0.0–0.3. The blue dashed line represents the location of the geotextile; the opening was located at the left side of the moisture contour plot.

Moisture Contours

The test started at 2:10 p.m. on July 13, 2016, and the moisture content within each testing box was recorded every 15 minutes. The saturation process started from S1 and ended at S3, and each testing box was fully saturated till extra water flowed out of the testing box. Figure 4.2 shows the moisture contours at the beginning of the test. Since the soil was loosely compacted, the hydraulic conductivity of the soil was expected to be relatively high. It can be seen from Figure 4.2(a) that the initial soil moisture content was not uniformly distributed, with higher value at the bottom and lower value at the top. Because S3 was the last box saturated, it showed the highest moisture condition among all three boxes. The highest water content for S2 and S3 was 0.31 and 0.25, respectively. Comparing the moisture contours for S1 and S3, the highest moisture content dropped to nearly half within 15 minutes for the same type of soil. This phenomenon indicates that the flow of water under gravity is a rapid process and can be completed in a short period. The Mechanistic-Empirical Pavement Design Method (MEPDG, 2009) recommends that if water can be removed from untreated base and subbase within 2 hours, the drainage condition can be rated as excellent. However, this method did not consider the amount of capillary water held within a pavement structure. How much water would be detained in the soil, or how much water cannot be drained by traditional drainage design was still a question that needed answering. If capillary water proves to be an equally important factor influencing pavement performance, it should be considered in the pavement subsurface drainage design.

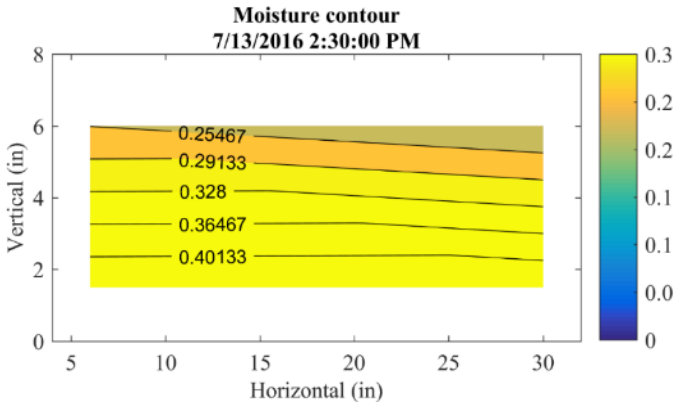

(a) Control box (S1)

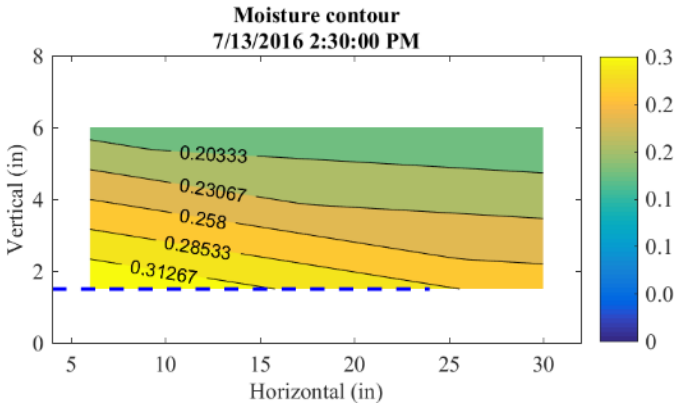

(b) Box with geotextile (S2)

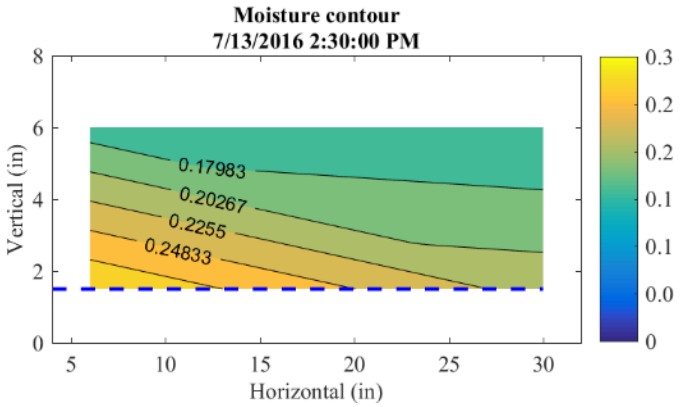

(c) Box with geotextile and grass (S3)

Figure 4.2 Moisture contours at starting point

Figure 4.3 shows the moisture contours for S1 through S3 one day after saturation. Even though the initial moisture condition within each testing box varied, the moisture condition for

each box should have been the same after completion of the saturation process. Thus, the moisture contours at this moment could be used to compare the moisture conditions in each box. As seen in Figure 4.3(a), geotextile was not installed in S1, and the moisture content on the left side of the box was higher than that on the right side. This phenomenon seemed unreasonable since the opening side was on the left and the moisture condition was expected to be lower on this side. However, since the testing box was seated on a slope with an angle of about 5° toward the left side, water was expected to drain from the right side to the left side. Moreover, the soil contained about 15% fines, which could absorb large amounts of capillary water, and capillary water could not be drained out of the testing box. Therefore, the accumulation of water on the left side of the box was caused by tilting, and the observation results were reasonable.

Figure 4.3(b) shows the moisture contour for S2 one day after saturation. The overall moisture condition for S2 was higher than for S1. The geotextile was supposed to wick capillary water out of the testing box, so the overall moisture condition of S2 should have been lower than that of S1. This phenomenon could be explained by two processes. First, the geotextile outside of the testing box was placed on top of a 2 in. thick layer of E-1 soil. Due to the extra E-1 material piled outside the testing box, the drainage holes located at the bottom of the testing box could not function well. This reduced the free water (water flow under the influence of gravity) drainage efficiency. Second, the authors maintained that high air suction caused the geotextile to cease working. However, even with the drainage holes blocked by E-1 soil, the wicking fabric should have been capable of wicking water out. Unfortunately, test results did not validate the authors' assertion. Due to the high suction (negative pore water pressure) value in the ambient environment (could be as high as 140 MPa), the air could easily break into the multi-channels of the wicking fiber and block the drainage paths. If large numbers of deep grooves in the wicking

fabric were occupied by air, the drainage efficiency of the geotextile might have been reduced or even might have caused the wicking fabric to stop working.

Figure 4.3(c) shows the moisture contour of S3 one day after saturation. The overall moisture condition for S3 was the lowest among all three testing boxes at this moment. Compared with S1, the highest moisture content was 0.15, which was 0.05 lower than S1. This indicated that the bio-wicking system worked effectively to wick extra capillary water out of the tested E-1 soil. Due to the existence of the revegetated grass, the geotextile was not directly exposed to the open air, and the topsoil served as a protective layer for the geotextile beneath it. On one hand, the grass on top of the bare soil impeded the evaporation process and maintained the moisture condition of the topsoil above the wilting point. According to the soil-water characteristic curve, a higher moisture content results in lower suction value. If the suction value of the soil near the geotextile layer was lower than the geotextile air entry value, air could not break into the multi-channels within the wicking fabric, and the deep grooves were in saturated condition to continuously wick water out of the testing box. On the other hand, the evapotranspiration process of the grass ensured that the excess capillary water wicked out of the testing box could be dissipated into the air. This process guaranteed that there always existed a suction gradient within and outside the testing box, which served as the potential force for water flow. Combining these two factors, the moisture condition in S3 was the lowest among all three testing boxes.

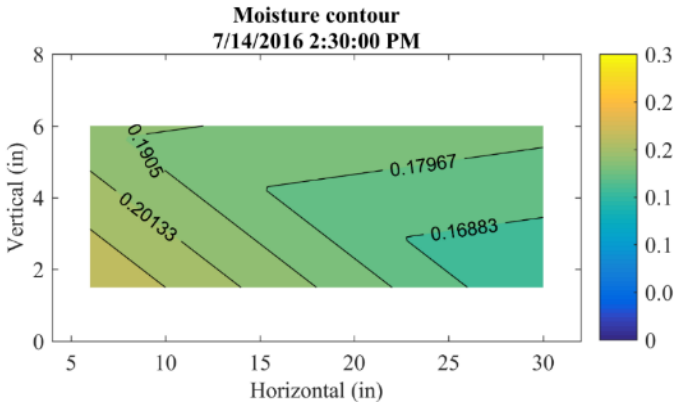

(a) Control box (S1)

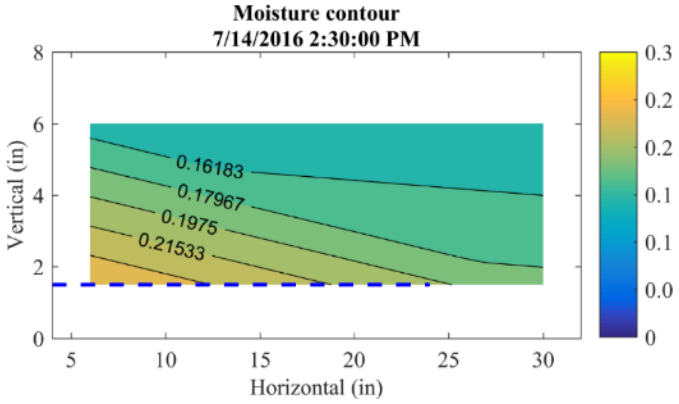

(b) Box with geotextile (S2)

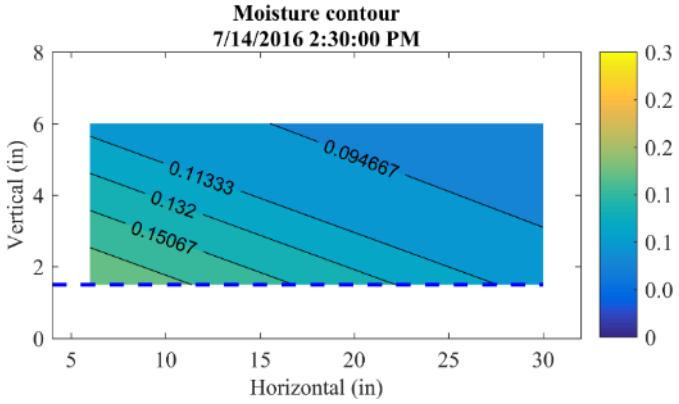

(c) Box with geotextile and grass (S3)

Figure 4.3 Moisture contours one day after saturation

Figure 4.4 shows the moisture contours of the testing boxes at the ending point.

Compared with the moisture contours for S1 in Figure 4.3, the moisture content distribution for

S1 (the control box) did not change on a large scale. The highest moisture content changed from 0.20 to 0.19, and the lowest moisture content changed from 0.17 to 0.16. After the rapid free-water draining process, capillary water could not be drained out effectively, and the amount of capillary water within the testing box ranged from 16% to 19% by volume. This comparison indicated that capillary water within the base course could be a critical factor influencing the pavement structure's long-term performance. A previous relevant project report (Lin and Zhang, 2016) indicated that only a 2% moisture content increment would result in the resilient modulus value of D1 material dropping to 1/3. Because base course provides major support to the traffic load above and is sensitive to moisture variations, it is very important to take capillary water into road drainage design.

For the test box with geotextile, the moisture distribution of S2 did not vary a lot compared with one day after saturation. The highest and lowest water content reduced to 0.15 and 0.20, respectively. This finding presented more evidence that the geotextile could not work effectively if directly exposed to the air. However, the bio-wicking system again showed the best performance among all three boxes. The highest moisture content was further reduced from 0.15 to 0.11, and the lowest moisture content was reduced to 0.06.

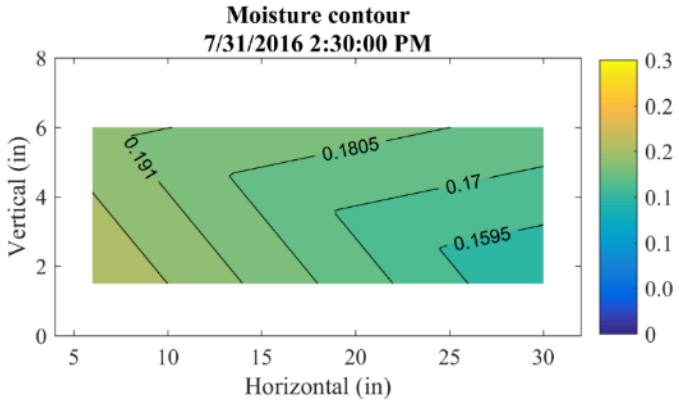

(a) Control box (S1)

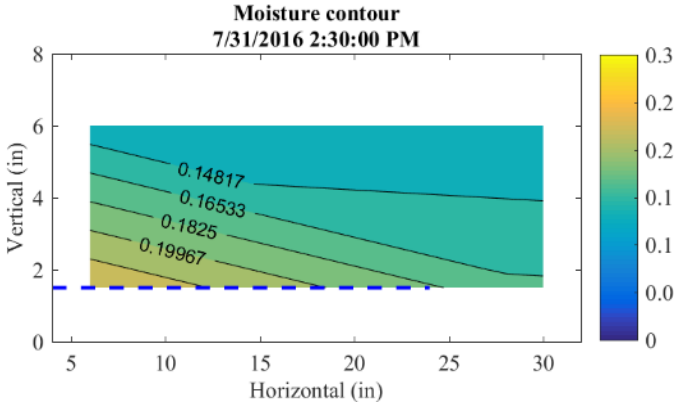

(b) Box with geotextile (S2)

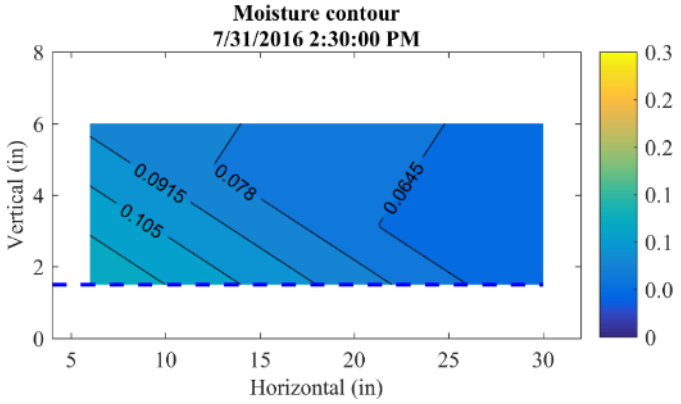

(c) Box with geotextile and grass (S3)

Figure 4.4 Moisture contours at ending point

Test Summary and Discussion

In addition to the moisture contours discussed in the previous section, the authors calculated the total amount of water within the testing boxes based on the recorded data. This calculation demonstrated the trend of water flow within the boxes, although the calculation only contained the area that four sensors could cover. Figure 4.5(a) shows the precipitation record during the testing period. In total, eight of the rainfall events exceeded 0.2 in.; two of them were even over 0.5 in.

Figure 4.5(b) shows the total volume of water detained in each testing box during the testing period. Since the construction process was finished on June 25, 2016, the geotextile

started to work two weeks before the test started. This is the reason why the initial volume of water in each testing flume was different. The initial volume of water within each testing flume could be considered as another indicator showing the effectiveness of the bio-wicking system. The testing soil for all three boxes was from the same batch and was expected to have minor moisture variations. This moisture condition represented the natural condition for E-1 soil. The volume of water within each testing box before testing was 4.43 L for S1, 3.44 L for S2 and 2.04 L for S3. These results indicate that the total volume of water was reduced to half for each box with the bio-wicking system. The bio-wicking system proved to be effective at wicking water out of the testing box.

By comparing the volume of water before and after saturation, the amount of water introduced to each testing box was approximately the same: all between 4.5 and 5 L. The amount of water that drained out within 2 hours from the starting point was 3.72 L for S1, 1.38 L for S2 and 2.09 L for S3. Since the drainage holes for S2 and S3 were blocked by the soils outside the box, the total amount of drained water was lower compared with S1. However, comparing the results of drained water from S2 and S3, one could clearly see that the bio-wicking system still drained more water than the box containing only geotextile.

It was not reasonable to compare the total water volume of each testing box after the test since the initial condition was not the same. However, the total amount of water detained in the box could be determined by observing the water volume difference before and after the test. This detained amount of water was considered an indicator of the drainage effectiveness of each case, which was 0.86 L for S1, 1.5 L for S2 and 0.38 L for S3. These results were consistent with the moisture contour observations discussed in the previous section. Moreover, the total amount of

detained water for S3 was still decreasing at a relatively high speed, which implied that the amount of water in S3 could be further decreased if longer testing time had been allowed.

Another interesting observation was that the fluctuation of total volume of water within the testing boxes was consistent with temperature variation in the soil. In Figure 4.5, the dashed line represents the air temperature recorded within the datalogger control panel, and the red solid line denotes the soil temperature within the testing box. There was a time lag for temperature variation within the testing box. Every increasing trend in air temperature would always coincide with soil temperature decreasing. Due to the insulating effect of soil, the amplitude of temperature fluctuations for soil was much smaller than for air temperature. Moreover, for each rainfall event, the fluctuation of air temperature also dramatically decreased. The soil temperature fluctuation would cause the variation of total volume of water detained in each testing box. High soil temperature, representing high potential energy, would result in low volume of water detained in the box. This phenomenon was observed for all three testing boxes.

In sum, the bio-wicking system showed the best drainage efficiency compared with the other two testing boxes. The relatively moist topsoil kept the soil suction lower than the geotextile air entry value, which ensured that the geotextile remained functional during the entire testing period. Moreover, the vegetation evapotranspiration process provided sufficient suction gradient as the driving force to continuously wick capillary water out of the testing box. Finally, the capillary water in E-1 materials should be considered in the drainage design because the E-1 material amounts to 18% of the total volume of soil.

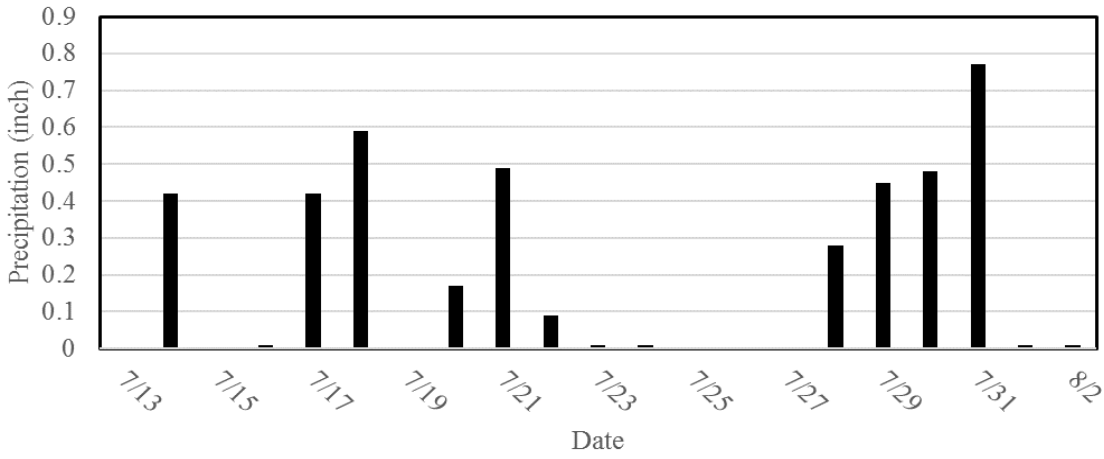

(a) Precipitation record

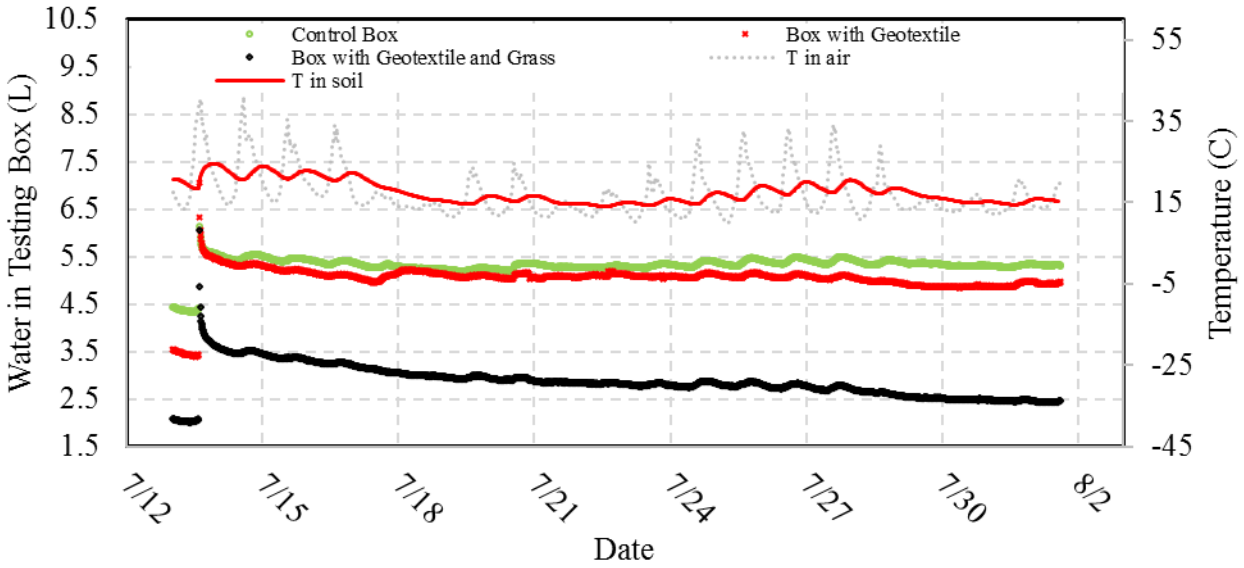

(b) Total volume of water within testing boxes

Figure 4.5 Elemental level test summary and discussion

4.2 Full-Scale Field Test Results

The full-scale field test started on July 25, 2016, and ended on October 2, 2016. This time two saturation operations were performed: the first on July 25 and the second on August 15. It is unnecessary to present the test results for all 10 testing flumes. The authors selected three typical flumes, Testing Flume 6, 8, and 10, to demonstrate bio-wicking system drainage efficiency.

Testing Flume 6 was the closest testing flume to the drainage ditch, which could be used to evaluate the effect of ambient environment on geotextile drainage efficiency. In Testing Flume 10, the geotextile was directly exposed to the air, which was the same as the small box S3 in the elemental level test.

Moisture Contours

Figure 4.6(a) shows the moisture contours for Testing Flume 6 during the first testing period. Similar to the elemental level small box test, the moisture distribution within the testing flume was not uniform due to the loose compaction of the soil and the relatively high hydraulic conductivity of the soil. Because the geotextile was only extended to 8 ft within the testing flume, the right end of the testing flume had higher moisture content than the left side. One day after saturation, the highest moisture content decreased from 0.38 to 0.23. The moisture content at the right side of the testing flume was still higher. At the left side of the testing flume, the moisture content was lower, indicating the water gradually flowed from right to left.

Figure 4.6(b) shows the moisture contours for Testing Flume 6 during the second testing period. During this test period, the data were recorded minutely for 2 hours and then recorded at a time interval of 15 minutes. The saturation process could be observed this time, as seen in the first image in Figure 4.6(b). On the right side of the testing flume, the moisture content was 0.41, indicating the soil was oversaturated. However, on the left side of the testing flume, the moisture content was much lower. Since the testing flume had an opening on the left end allowing exposure of the geotextile to the outside, the free water could easily flow out of the flume. One day after the second saturation, the moisture content at 40 in. horizontally was higher, and the highest moisture content dropped from 0.41 to 0.25. At the end of the test, the moisture content

at 40 in. rose higher. This phenomenon was caused by rainfall events, which will be explained in detail later.

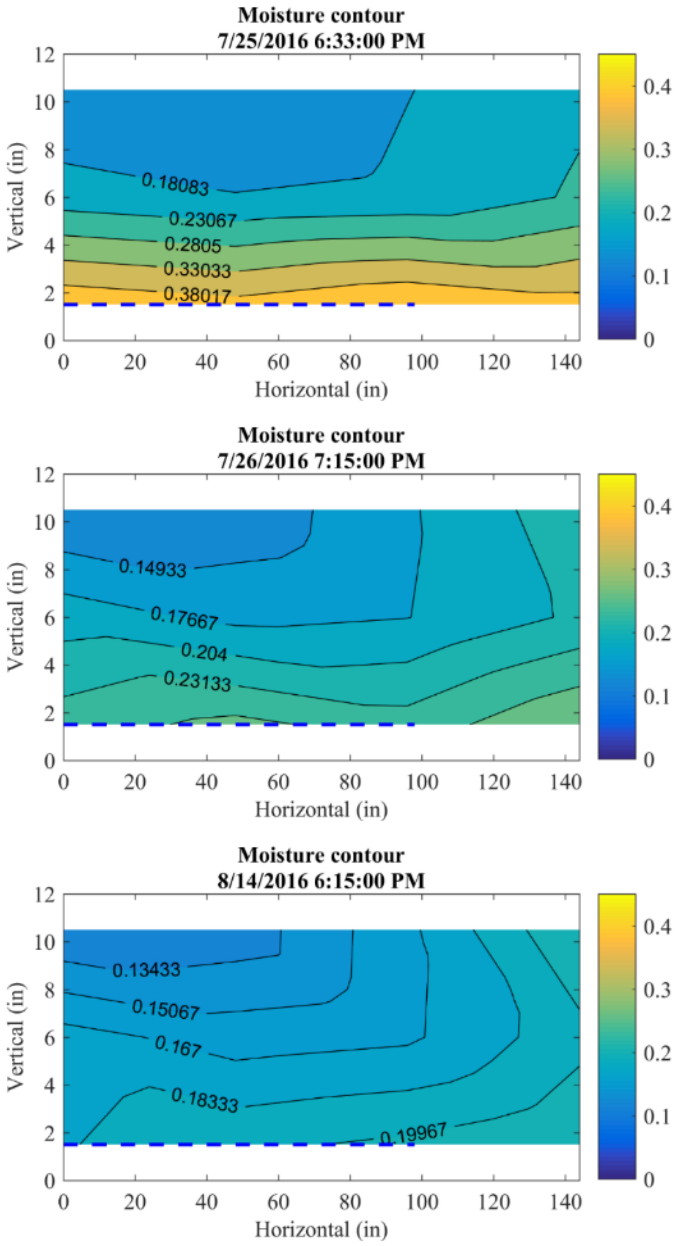

(a) 1st testing period

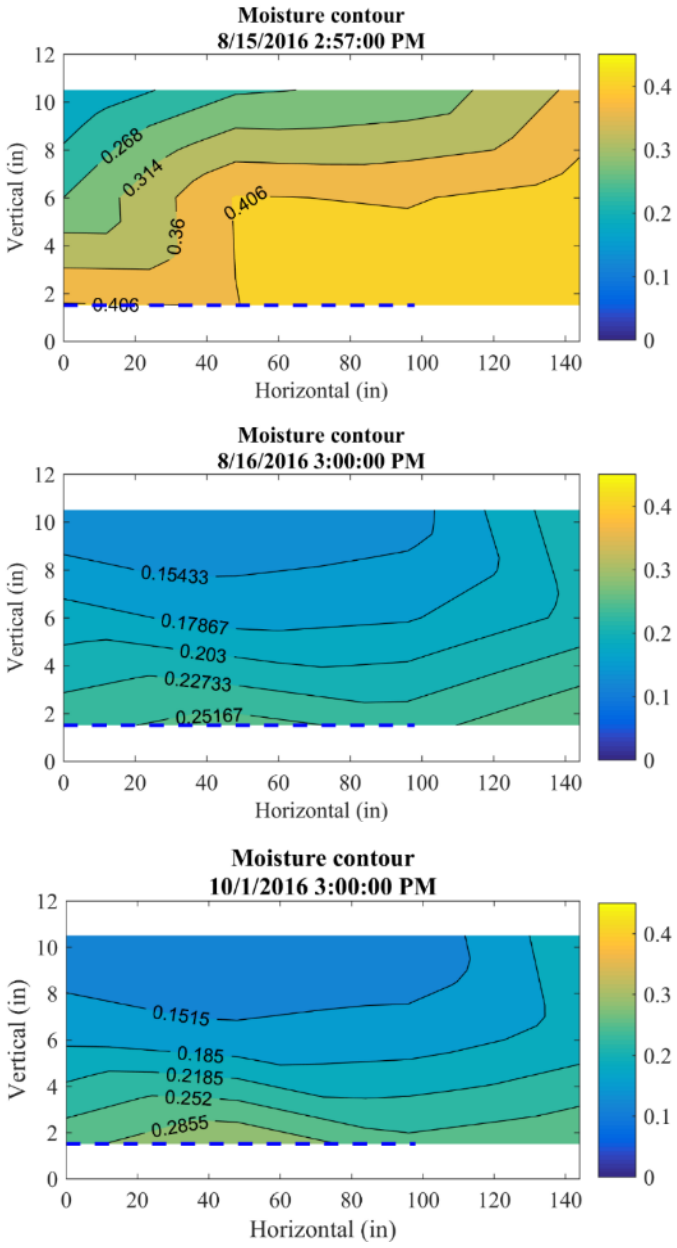

(b) 2nd testing period

Figure 4.6 Testing Flume 6

Figure 4.7 shows the moisture contours of Testing Flume 8 during the first and second testing period. Unlike Testing Flume 6, the moisture content distribution was abnormal at the beginning of the test. The lowest moisture content was observed in the middle of the testing flume, which might have been caused by inconsistency during the compaction process. Because

the recorded air temperature was always above 0°C, the lower moisture content was not induced by capillary action. One day after saturation, the middle layer experienced even lower moisture content. During the first 18 days of the testing period, the highest moisture content dropped from 0.20 (one day after saturation) to 0.17. The bio-wicking system was working, and the drainage efficiency was higher than Testing Flume 6.

Figure 4.6(b) shows the moisture contours for Testing Flume 8 during the second testing period. The highest moisture content dropped from 0.46 to 0.21 within one day after saturation, and the lowest moisture content was observed in the middle layer. Moreover, the moisture distribution did not vary much during the second test, and the average moisture content dropped to 0.16.

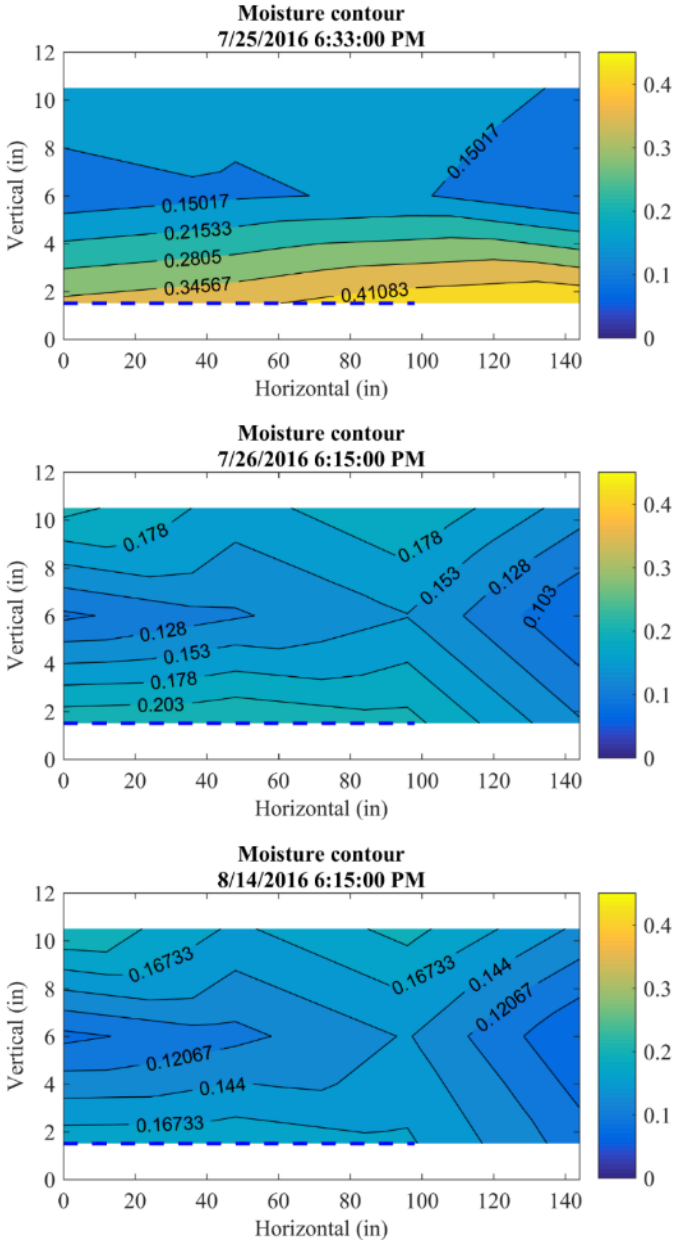

(a) 1st testing period

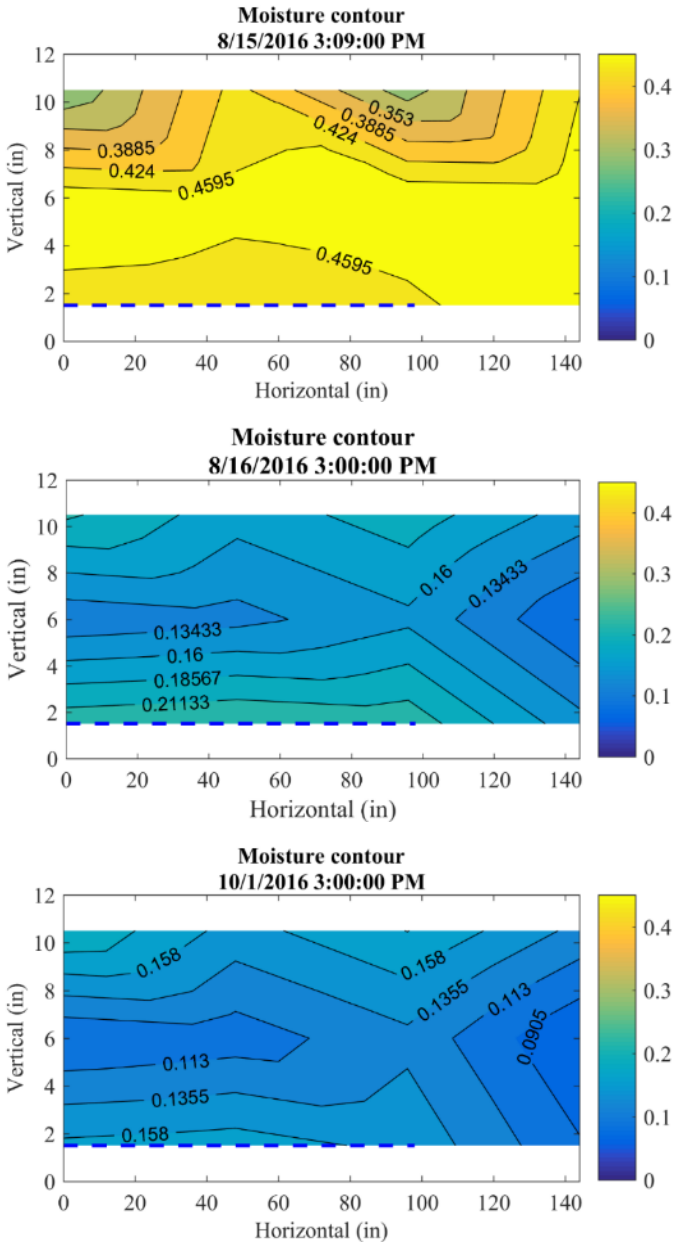

(b) 2nd testing period

Figure 4.7 Moisture contours for Testing Flume 8

Figure 4.8 shows the moisture contours for Testing Flume 10. The highest moisture content was 0.40 at the beginning of the first testing period and dropped to 0.26 at the right side of the flume. In addition, the highest moisture content was observed at the bottom of the left side of the flume, indicating that the geotextile did not work effectively at wicking water out of the

testing flume. Again, as explained in the discussion on the elemental level box, the drainage efficiency of the geotextile was significantly reduced owing to air breaking into the multi-channels of the wicking fibers. At the end of the first testing period, there was an area with higher moisture content concentration (0.20), and the overall moisture content was the highest among all three testing flumes. Both elemental level and full-scale tests indicated that geotextile exposed to the air would not work effectively to wick water out of the box/flume. In contrast, the bio-wicking system was the most effective combination.

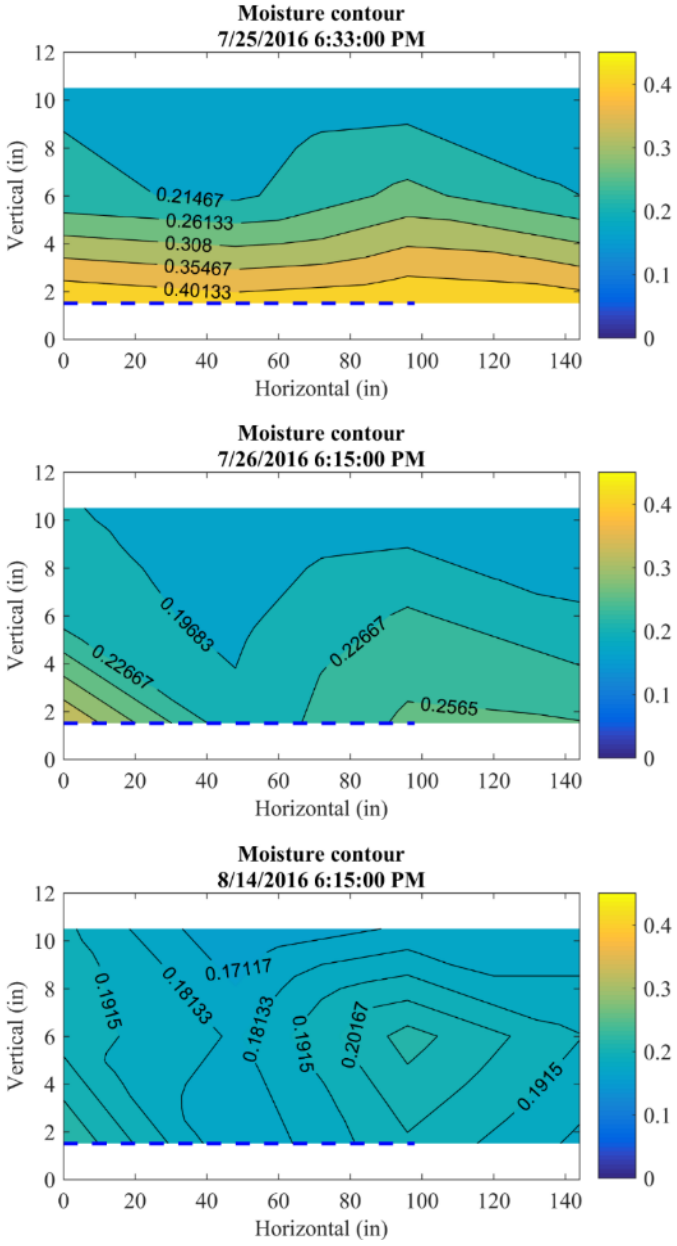

(a) 1st testing period

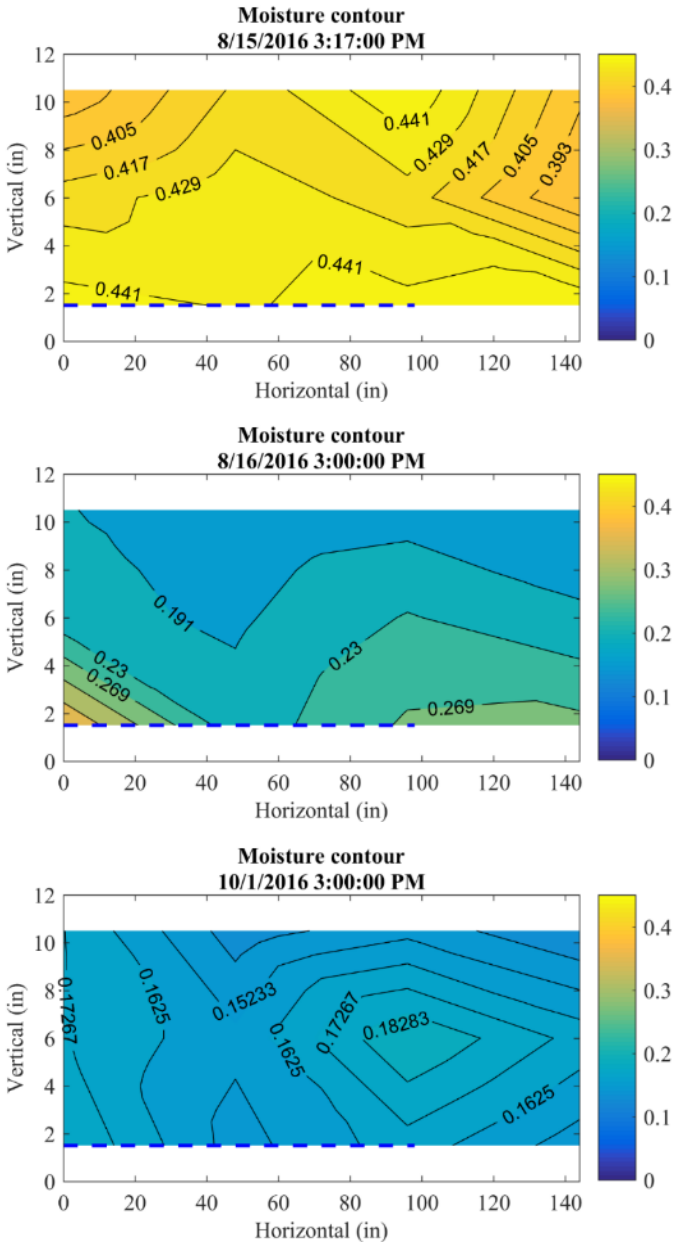

(b) 2nd testing period

Figure 4.8 Moisture contours for Testing Flume 10

Test Summary and Discussion

Figure 4.9 shows a summary of the field full-scale test results. Figure 4.9(a) indicates the precipitation data during the testing period. There were ten rainfall events with precipitation higher than 0.2 in.

Figure 4.9(b) shows the total volume of water detained within each testing flume. The effect of precipitation was significant on the total volume of water for Testing Flume 6. Since Testing Flume 6 was the closest to the drainage ditch, it was reasonable to observe such large variations of total volume of water within the testing flume. Furthermore, the total volume of water rose suddenly after each heavy precipitation. This phenomenon indicated that the water flowed back into the testing flume during the heavy rainfall events. However, in comparing Testing Flumes 10 and 6, the total volume of water for Testing Flume 10 did not indicate any sudden and significant increment. Because the geotextile was exposed to the air, the geotextile could neither effectively wick water out of the testing flume, nor transport water into the testing flume. Even though the total volume of water within Testing Flumes 6 and 8 varied throughout the test, the total volume of water within Testing Flume 10 was still the highest if accounting for the amount of water that flowed into Testing Flume 6.

In sum, the bio-wicking system worked effectively in laterally transporting water out of the testing flume compared with the testing flume only with geotextile. However, the bio-wicking system was sensitive to heavy rainfall events, resulting in water flowing in the reverse direction and increasing the total amount of water in the testing flume.

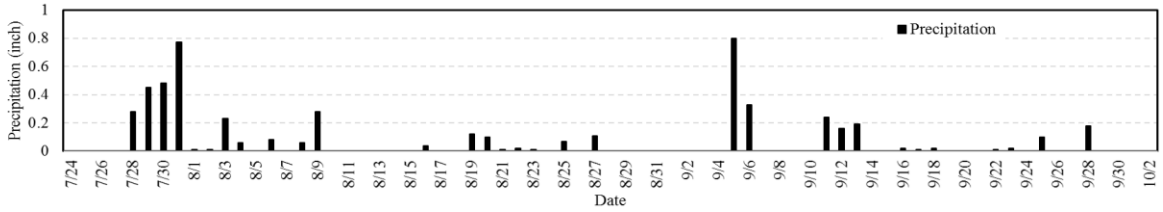

(a) Precipitation record

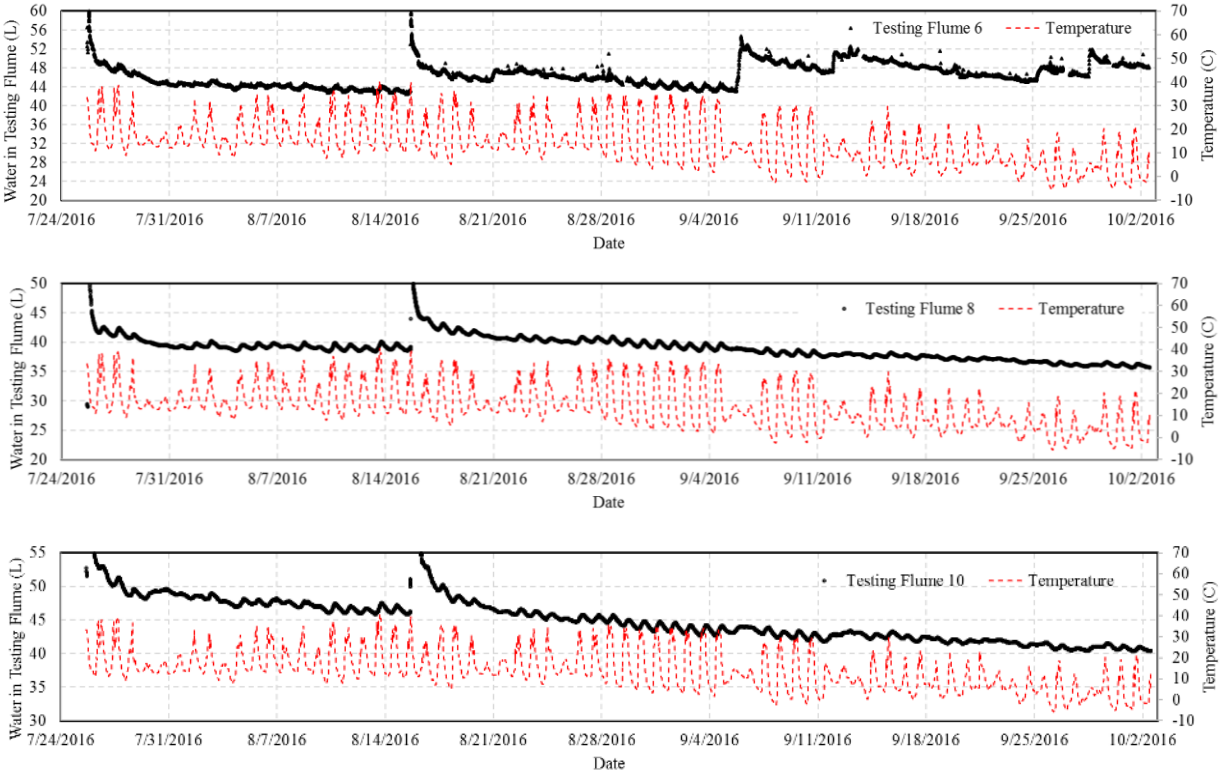

(b) Total volume of water

Figure 4.9 Field full-scale test summary and discussion

As discussed before, the air entry value of the geotextile was an important factor in determining the functional range of the geotextile. In order to determine the geotextile air entry value, a lab test was proposed by the authors as shown in Figure 4.10(a). The testing equipment was modified from the one-dimensional consolidation equipment. The geotextile was sandwiched by two layers of saturated Fairbanks silt. At the bottom of the soil layer, a high

suction torsiometer was used to measure suction variations. It was considered that if the soil-geotextile reached equilibrium, the suction of the soil was the same as that within the geotextile.

Figure 4.10(b) shows the test results. In total, three tests were performed with different initial moisture contents and loading level. A comparison of the test results for Test 1 and Test 2 indicated that the initial moisture content did not significantly influence the geotextile. The slopes of suction over time decreased considerably after 45 hours and gradually approached equilibrium. Moreover, loading accelerated the water dissipation process, but did not affect the geotextile air entry value (Comparison of Test 1 and Test 3). For Test 3, 150 kPa of external load was applied on top of the consolidation ring, and the soil-geotextile system reached equilibrium at 35 hours. In sum, the air entry value of the geotextile was approximately 40–45 kPa. The air entry value was not sensitive to the soil/geotextile initial moisture condition and external loading.

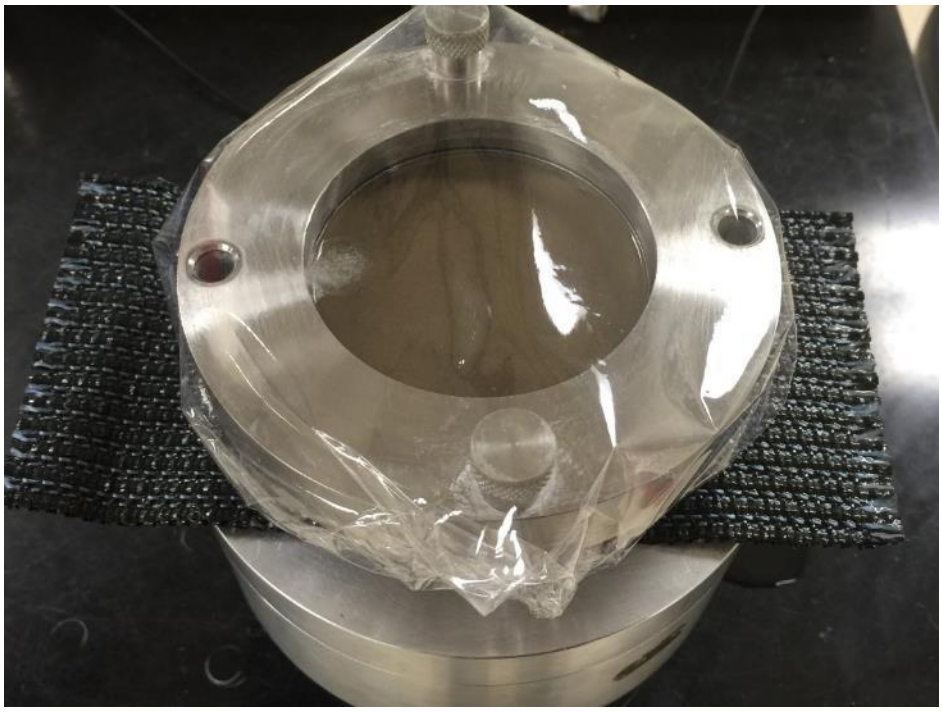

(a) Testing equipment

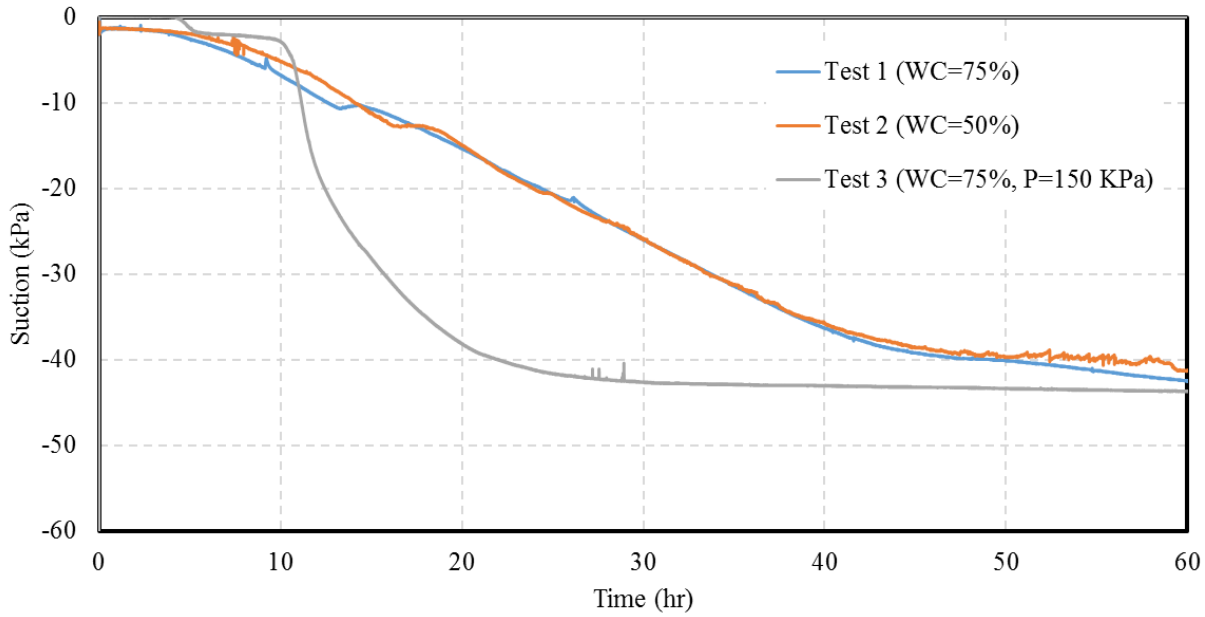

(b) Test results

Figure 4.10 Geotextile air entry value determination

4.3 Geotextile-Grass Interactions

As demonstrated in the elemental-level and full-scale tests, the bio-wicking system showed the best drainage performance among all three cases. In this section, the interaction between the grass and the geotextile is discussed, and the working mechanism of the bio-wicking system is explained.

Figure 4.11 is a macroscopic view of the grass-geotextile interaction, showing a small section of the geotextile buried beneath the topsoil with vegetation at the top. The photograph clearly shows that the grass roots grew downward and penetrated the geotextile layer. The geotextile was in good contact with the grass roots, which ensured good water-transporting channels between two different materials. The capillary water wicked out of the testing box/flume was available for the grass evapotranspiration process. Figure 4.11(b) shows the top view of the backside of the geotextile after the topsoil near the grass roots was carefully

removed. This figure further proves the interlaced texture between the geotextile and the grass roots. The grass roots were grown randomly without preference to weaving or cross machine directions.

(a) Section of bio-wicking system for element level test

(b) Grass roots penetrating the geotextile

Figure 4.11 Grass-geotextile interaction (macroscopic view)

Figure 4.12 shows the intact geotextile with dry grass roots after the geotextile was pulled from the test section. The geotextile was buried 2 in. beneath the soil surface, and the topsoil on the geotextile surface was washed away for microscopic analyses. The grass roots had intruded into the geotextile weaving yarns. The spacing and gaps between the white wicking yarns and black reinforcement yarns are relatively large so that the grass roots had easy access and good contact with the wicking yarns.

Figure 4.12 Microscopic image of grass-geotextile interaction

Part of the sample in Figure 4.12 was used to further examine the interactions of grass and geotextile using a scanning electron microscope (SEM), as shown in Figure 4.13. Figure 4.13(a) shows the SEM image of the grass root closer to the stem. The cutaway image indicates high similarity between the deep grooved structure of the grass root and the artificially designed multi-channel of the geotextile wicking fabric. The spacing of the grooves in the grass root was about 10 microns, similar to the spacing of the wicking fabric. The grass and the geotextile share the same working mechanism in transporting water. The transpiration process of the grass was driven in part by capillary action and water potential difference (Zhu and Zhang, 2015). If the

water potential in ambient air is lower than the water potential in the grass leaf airspace of the stomatal pore, water travels down the gradient and moves from the leaf airspace to the atmosphere via the evaporation process. Therefore, evapotranspiration is the sum of evaporation and transpiration of the entire water cycle within a plant. Similarly, water transportation within the wicking fabric is driven by capillary action or by water potential difference (suction gradient) between the two ends of the geotextile. In sum, the bio-wicking system is essentially a combination of two drainage materials sharing the same working mechanism that transports water under the influence of capillary action.

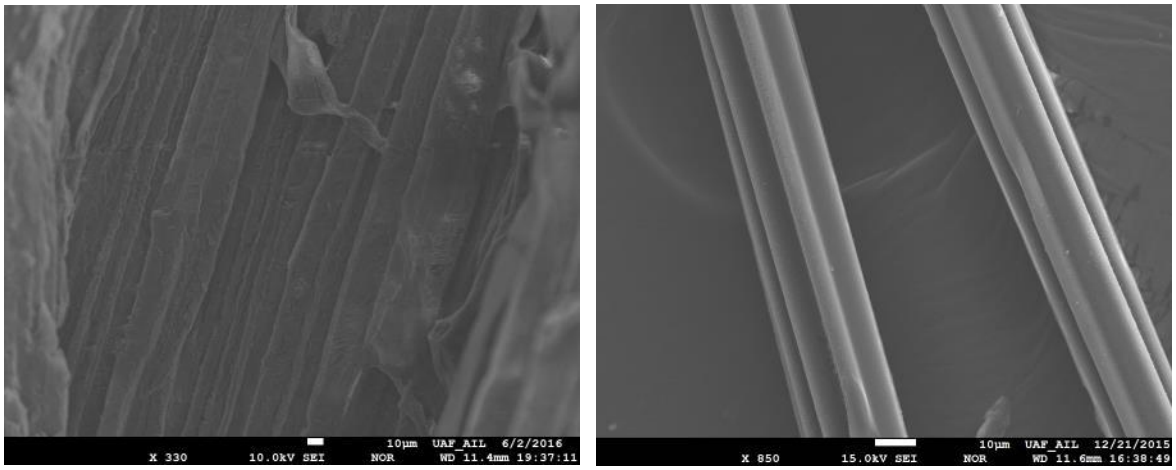

(a) Grass root (b) Wicking fabric

Figure 4.13 Similarities between grass root and geotextile wicking fabric

CHAPTER 5.0 CONCLUSIONS

This project's focus was the possibility of using a bio-wicking system to mitigate moisture conditions within unbound base course. Both elemental level and full-scale field tests proved that the bio-wicking system is efficient at reducing capillary water within the base course. The major conclusions drawn from the test results are as follows:

1. In the elemental level test, capillary water consisted of at least 1/3 of the total water introduced to each testing box. This part of the water was considered undrainable in conventional subsurface drainage designs. Moreover, the moisture content within the testing flume varied in accordance with the ambient temperature. This test indicated that capillary water is equally as important a factor as free water in determining pavement performance in the long run and should be considered in the drainage design.
2. The bio-wicking system is a more effective design in mitigating capillary water within the base course than the previous design with geotextile directly exposed to the open air. Both elemental level and full-scale field tests proved that moisture content in the testing box/flume with the bio-wicking system was the lowest. The moisture contours for the testing flume with geotextile exposed to the air clearly showed that the geotextile stopped working several days after the second saturation was completed. In contrast, the testing flume with the bio-wicking system continuously wicked water out of the flume, and more capillary water would have drained out if a longer test time had been allowed (the total volume of water continued to decrease after the test was finished).

3. The air entry value of geotextile is a critical factor in determining when the geotextile will stop working. If the ambient suction value exceeds the geotextile air entry value, hydraulic conductivity will significantly decrease and the geotextile will stop working. At this moment, the geotextile serves as a layer of capillary barrier rather than a drainage material. Therefore, it is critical to maintain the suction of the surrounding soil under the geotextile air entry value.
4. The vegetation of the bio-wicking system reduces the evaporation rate of the soil beneath it and ensures that the geotextile serves as a drainage material. On the other hand, the vegetation transpiration process continuously wicks water out of the soil in the form of water vapor. This evapotranspiration process guarantees that the geotextile continuously functions as drainage material, constantly reducing the amount of capillary water in the base course.
5. The microscopic analysis of the grass-geotextile interaction further validated the working mechanism of the bio-wicking system. The similarities of the grass and geotextile microstructures indicated that the essential working mechanisms for grass and geotextile are the same. Both of them take advantage of capillary action and water potential difference (suction gradient) to transport water. There are two similar processes in the bio-wicking system: the geotextile first wicks water out of the base course to the soil, and then vegetation further wicks water to the grass leaf and evaporates it in the air via the transpiration process.

In addition to these conclusions, the following are several recommendations for future application of geotextiles:

1. The geotextile should be buried deeper than described in this project. The buried depth in this project was 1–2 in. to make sure the grass roots could have good contact with the geotextile wicking fabrics. However, microscopic analysis showed that the grass roots penetrated the geotextile and kept growing downward. The average grass root length was over 5 in.; thus, the geotextile can safely be buried to this depth in future applications.
2. Precipitation has an impact on bio-wicking system drainage efficiency. Heavy rainfall events will oversaturate the top layer of the bio-wicking system and result in higher moisture content. If the moisture content of the bio-wicking system is higher than that of the base course, the water will transport in a reverse direction and increase the moisture content of the base course. Test results indicate that precipitation higher than 0.2 in. will cause this scenario. Therefore, application of the bio-wicking system in an area of high precipitation will require more attention to this issue.
3. The process of capillary water transport is a slow process compared with free water movement. Free water can be quickly drained out of base course within two hours, while capillary water drainage takes several weeks or even months. The efficiency of the bio-wicking system cannot be observed in a relatively short period. Therefore, if further research is required to evaluate the effectiveness of the bio-wicking system, the monitoring process should be lengthened to several months, or even several years.

REFERENCES

Allen, R.G., Pereira, L.S., Raes, D., and Smith, M. (1998). "Crop evapotranspiration guidelines for computing crop water requirements." FAO Irrigation and Drainage Paper 56, Food and Agriculture Organization of the United Nation.

Aravin, V.I., and Numerov, S.N. (1953). "Theory of motion of liquids and gases in undeformable porous media." Israel Program for Scientific Translation, Jerusalem.

Barber, E.S., and Sawyer, C.L. (1952). "Highway sub-drainage." Proceedings, Highway Research Board, 31, 642–666.

Bathurst, R.J. (2007). "Geosynthetics classification." IGS Leaflets on Geosynthetics Applications, IGS Education Committee, available at *www.geosyntheticssociety.org*

Bathurst, R.J., and Raymond, G.P. (1987). "Geogrid reinforcement of ballasted track." *Transportation Research Record*, No. 1153, 8–14.

Baumgartner, A., and Reichel, E. (1975). *The world water balance-mean annual global, continental, and maritime precipitation, evaporation, and run-off.* Elsevier: Amsterdam, The Netherlands, 179 pp.

Benjamin, C.V., Bueno, B., and Zornberg, J.G. (2007). "Field monitoring evaluation of geotextile reinforced soil retaining walls." *Geosynthetics International Journal*, 14(2), 100–118.

Beskow, G. (1991). "Reprinted in historical perspectives in frost heave research" (P.B. Black and M.J. Hardenberg, eds.). *CRREL Special Report*, No. 91–23, 37–157.

Bueno, B.S., Benjamim, C.V., and Zornberg, J.G. (2005). "Field performance of a full-scale retaining wall reinforced with non-woven geotextiles." Slopes and Retaining Structures

under Seismic and Static Conditions, *ASCE GSP No. 140*, January, Austin, Texas (CD-ROM).

Casagrande, A. (1947). "Classification and identification of soils." Proceedings, American Society of Civil Engineers, 73(6), 283.

Cedergren, H.R. (1974). *Drainage of highway and airfield pavements*. John Wiley & Sons, Inc.: NY.

Cedergren, H.R. (1994). "America's pavements: world's longest bathtubs civil engineering." *American Society of Civil Engineering*, 64(9), 56–68.

Cedergren, H.R., O'Brien, K.H., and Arman, J.A. (1973). "Guidelines for the design of subsurface drainage systems for highway structural sections." Federal Highway Administration, Final Report Number FHWA-RD-73-14, Washington, D.C.

Chamberlain, E.J. (1987). "A freeze-thaw test to determine the frost susceptibility of soils." U.S. Army Corps of Engineers, *CRREL Special Report*, 87-1.

Christopher, B.R., and McGuffey, V.C. (1997). "NCHRP synthetics of highway practice 239: Pavement subsurface drainage systems." Transportation Research Board, National Research Council, Washington, DC.

Christopher, B.R., Hayden, S.A., and Zhao, A. (2000). "Roadway base and subgrade geocomposite drainage layers." Proceedings, Testing and Performance of Geosynthetics in Subsurface Drainage, Seattle, Washington, 35–51.

Collin, J.G. (1996). "Controlling surficial stability problems on reinforced steepened slopes." Geotechnical Fabrics Report, Industrial Fabrics Association International, St. Paul, MN, April.

Coppin, N.J., and Richards, I.G. (1990). "The use of vegetation in civil engineering." Construction Industry Research & Information Association (CIRIA), Lincoln, UK.

Csathy, T.I., and Townsend, D.L. (1962). “Pore size and field frost performance of soils.” *Highway Research Board Bulletin*, No.331, 67–80.

Dingman, S.L. (1992). *Physical hydrology*. Prentice Hall: Upper Savage, New Jersey.

Giroud, J.P., Ah-Line, C., and Bonaparte, R. (1984). “Design of unpaved roads and trafficked areas with geogrids.” Conference, Polymer Grid Reinforcement, Thomas Telford, London, England, 116–127.

Giroud, J.P., and Noiray, L. (1981) “Geotextile-reinforced unpaved road design.” *Journal of Geotechnical Engineering, ASCE*, 107, 1233–1254.

Han, J., and Guo, J. (2015). “Geosynthetic-stabilized vegetated earth surfaces for environmental sustainability in civil engineering.” Innovative Materials and Design for Sustainable Transportation Infrastructure, American Society of Civil Engineers, 276–285.

Han, J., and Thakur, J.K. (2014). “Sustainable roadway construction using recycled aggregates with geosynthetics.” *Sustainable Cities and Society*, 14, 342–350.

Han, J., and Zhang, X. (2014). “Recent advances in the use of geosynthetics to enhance sustainability of roadways.” 20th International Conference on Advances in Civil Engineering for Sustainable Development, Suranaree University of Technology, Nakhon Ratchasima, Thailand, 29–39.

Heckel, L. (1997). “Performance problems of open-graded drainage layers under continuously reinforced concrete pavement in Illinois.” *Transportation Research Record, 1596,* National Research Council, Washington, DC, 51–57.

Henry, K.S. (1998). “Use of geotextiles to mitigate frost heave in soils.” Proceedings, 5th International Conference on Permafrost, Trondheim, Norway, 1096–1011.

Henry, K.S., and Holtz, R.D. (1997). "Capillary rise of water in geotextiles." Proceedings, International Symposium on Ground Freezing and Frost Action in Soils, Lulea, Sweden, 227–233.

Henry, K.S., and Stormont, J.C. (2002). "Geocomposite capillary barrier drain for limiting moisture changes in pavement subgrades and base courses." NCHRP-IDEA 68 Final Report, Transportation Research Board, Washington, DC.

Henry, K.S., Stormont, J.C., Barna, L.A., and Ramos, R.D., (2002). "Geocomposite capillary barrier drain for unsaturated drainage of pavements." Proceedings, 7th International Conference on Geosynthetics, Nice, France, 3, 877–880.

Holtz, R.D, Christopher, B.R., and Berg, R.R. (1998). "Geosynthetics design and construction guidelines." Federal Highway Administration, Washington, DC, FHWA-HI-98-038, 460.

Khing, K.H., Das, B.M., Puri, V.K., Cook, E.E., and Yen, S.C. (1993). "The bearing capacity of a strip foundation on geogrid reinforced sand." *Geotextiles and Geomembranes*, 12, 351–361.

Kochina, P., and Ya, P. (1952). "Theory of motion of ground water." Moscow: Gosudarstv. Izdat. Tehn.-Teor. Lit., translated as Polubarinova-Kochina, P. Ya., 1962. *Theory of ground water movement*. Princeton University Press: Princeton, NJ.

Krisdani, H., Rahardjo, H., and Leong, E.C. (2008). "Measurement of geotextile-water characteristic curve using capillary rise principle." *Geosynthetics International*, 15(2), 86–94.

Lane, K.S., and Washburn, S.E. (1946). "Capillary tests by capillarimeter and by soil filled tubes." *Highway Research Board, 26, Transportation Research Board*, Washington, DC, 460–473.

Li, J., Okin, G.S., Hartman, L.J., and Epstein, H.E. (2007). "Quantitative assessment of wind erosion and soil nutrient loss in desert grasslands of southern New Mexico, USA." *Biogeochemistry*, 85, 317–332.

Lin, C., and Zhang, X. (2016). "Development of design method for h2ri wicking fabric in pavement structures." Alaska University of Transportation Center (AUTC), Project Report. (Under Review).

Lin, C., and Zhang, X. (2016). "Development of design method for H2Ri wicking fabric in pavement structures." *Alaska University Transportation Center (AUTC)*, University of Alaska Fairbanks, Fairbanks, AK., (under review)

Loch, R.J. (2000). "Effects of vegetation cover on runoff and erosion under simulated rain and overland flow on a rehabilitated site on the Meandu Mine, Tarong, Queensland. Australian." *Journal of Soil Resources*, 38, 299–312.

Mallela, J., Titus-Glover, L., and Darter, M.I. (2000). "Considerations for providing subsurface drainage in jointed concrete pavements." *Transportation Research Record 1709*, National Research Council, Washington, DC, 1–10.

McMahon, T.A., Peel, M.C., Lowe, L., Srikanthan, R., and McVicar, T.R. (2013). "Estimating actual, potential, reference crop and pan evaporation using standard meteorological data: a pragmatic synthesis." *Hydrology and Earth System Science*, 17, 1331–1363.

Mechanistic-Empirical Pavement Design Guide, *http://www.trb.org/mepdg/home.htm*, Last Accessed: Jan 2017.

Miller, R.D. (1978). "Frost heaving in non-colloidal soils." In Proceedings of the Third International Conference on Permafrost, July 10-13, 1978, Edmonton, Alberta, Volume 1, Ottawa, Ont., *National Research Council of Canada*, 708-713.

Monteith, J. L. (1965). “Evaporation and environment” in: *The state and movement of water in living organisms*. Symposium Society Experimental Biology, Cambridge University Press: London, 19, 205–234.

Monteith, J.L. (1991). “Weather and water in the Sudano-Sahelian zone.” Proceedings, Niamey Workshop, February, IAHS Publication No. 199.

Moosmuller, H., Gillies, J.A., Rogers, C.F., DuBois, D.W., Chow, J.C., and Watson, J.G. (1998). “Particulate emission rates for unpaved shoulders along a paved road.” *Journal of the Air & Waste Management Association*, 48, 398–407.

Morgan, R. P. C. (1995). *Soil erosion and conservation*, 2nd ed. Longman, Harlow, 198 pp.

Morgan, R.P.C., and Rickon, R.J. (2003). *Slope stabilization and erosion control: A bioengineering approach*. E & Fn Spon, 2-6 Boundary Row, London, SE1 8HN.

Morgan, R.P.C., and Rickson, R.J. (1995). “Slope stabilization and erosion contrl: a bioengineering approach.” *E&F Spon, London*, England.

Muller W.W., and Saathoff, F. (2015). “Geosynthetics in geoenvironmental engineering.” *Science and Technology of Advanced Materials*, 16(3), 20.

Muskat, M. (1937). *The flow of homogeneous fluids through porous media.* McGraw-Hill Book Co.: NY, London.

Niroumand, H., and Millona, K. (2010). “Mud bricks and shred geogrids as sustainable material.” *Geotechnical News*, 28 (4), 59–61.

Palmeira, E.M., Tatsuoka, F., Bathurst, R.J., Stevenson, P.E. and Zornberg, J.G. (2008). "Advances in Geosynthetics Materials and Applications for Soil Reinforcement and Environmental Protection Works", *Electronic Journal of Geotechnical Engineering*, Special Issue Bouquet 08.

Peng, F-L., Kotake, N., Tatsuoka, F., Hirakawa, D., and Tanaka, T. (2000). "Plane strain compression behaviour of geogrid-reinforced sand and its numerical analysis." *Soils and Foundations*, 40(3), 55–74.

Penman, H.L. 1948. "Natural evaporation from open water, bare soil and grass." Proceedings, Royal Society of London. Series A, Mathematical and Physical Sciences, 193(1032), 120–145.

Perkins, S.W., and Ismeik, M. (1997a). "A synthesis and evaluation of geosynthetics-reinforced base course layers in flexible pavements: Part I, experimental work." *Geosynthetics International*, 4(6), 549–604.

Perkins, S.W., and Ismeik, M. (1997b). "A synthesis and evaluation of geosynthetics-reinforced base course layers in flexible pavements: Part II, analytical work." *Geosynthetics International*, 4(6), 605–621.

Potyondy, D., Siekmeier, J., and Petersen, L. (2016). "Aggregate-geogrid interaction model incorporating moisture effects." (Accepted in *Transportation Research Board*, 2016).

Qian, Y., Mishra, D., Tutumluer, E., and Kwon, J. (2013). "Comparative evaluation of different aperture geogrids for ballast reinforcement through triaxial testing and discrete element modeling." *Geosynthetics*, April 1–4, Long Beach, CA.

Shuttleworth, W.J. (1992). *Handbook of hydrology* (D.R. Maidment, ed.). McGraw-Hill Inc.: NY.

Stockton, T.B. (2001). "Performance experimental testing of diversion lengths for a geocomposite unsaturated drainage system." M.S. thesis, University of New Mexico, Albuquerque, NM.

Stormont, J.C., Henry, K.S., and Evans, T.M. (1997). "Water retention functions of four nonwoven polypropylene geotextiles." *Geosynthetics International*, 4 (6), 661–672.

Stormont, J.C., Henry, K.S., and Roberson, R. (2009). “Geocomposite capillary barrier drain for limiting moisture changes in pavements: Product application.” Transportation Research Board, National Cooperative Highway Research Program, NCHRP-113.

Stormont, J.C., Ray, C., and Evans, T.M. (2001). “Transmissivity of a nonwoven polypropylene geotextile under suction.” *ASTM Geotechnical Testing Journal*, 24(2), 164–171.

Taber, S. (1930a). “The mechanics of frost heaving.” *Journal of Geology*, 38, 303–317.

Taber, S. (1930b). “Freezing and thawing of soils as factors in the destruction of road pavements.” *Public Roads*, 11(6), 113–132.

Takagi, S. (1978). “Segregation freezing as the cause of suction force in ice lens formation.” *Cold Regions Research and Engineering Laboratory (CRREL)*, Report No. 78-6, 12.

TenCate Geosynthetics North America (2010). “Geosynthetic reinforcement of the aggregate base/subbase courses of pavement structures.” TenCate Geosynthetics North America, Technical Note.

Wright, S.J. (2008). “A revegetation manual for Alaska.” Alaska Plant Materials Center, Division of Agriculture, Alaska Department of Natural Resources.

Zheng, F. (2006). “Effect of vegetation changes on soil erosion on the Loess Plateau.” *Pedosphere*, 16(4), 420–427.

Zhu, H., and Zhang, L. (2015). “Evaluating suction profile in a vegetated slope considering uncertainty in transpiration.” *Computers and Geotechnics*, Vol. 1, 112-120.

Zornberg, J.G., and Mitchell, J.K. (1994). “Reinforced soil structures with poorly draining backfills. Part I: Reinforcement interactions and functions.” *Geosynthetics International*, 1(2), 103–147.